Journal of Medicinal Chemistry

pubs.acs.org/jmc

Article

Synthesis and Evaluation of Galloyl Conjugates of Flavanones as BMP-2 Upregulators with Promising Bone Anabolic and Fracture Healing Properties

Alka Raj Pandey,[▽] Divya Rai,[▽] Suriya Pratap Singh, Ashish Kumar Tripathi, Anirban Sardar, Alisha Ansari, Anjali Mishra, Sudha Bhagwati, Rabi Sankar Bhatta, Mohammad Imran Siddiqi, Naibedya Chattopadhyay, Ritu Trivedi,* and Koneni V. Sashidhara*

Cite This: https://doi.org/10.1021/acs.jmedchem.1c00112

Read Online

ACCESS | Metrics & More | Article Recommendations | Supporting Information

ABSTRACT: The molecular hybridization concept led us to design a series of galloyl conjugates of flavanones that have potent osteoblast differentiation ability *in vitro* and promote bone formation *in vivo*. An array of *in vitro* studies, especially gene expression of osteogenic markers, evinced compound **5e** as the most potent bone anabolic agent, found to be active at 1 pM, which was then further assessed for its osteogenic potential *in vivo*. From *in vivo* studies on rat calvaria and a fracture defect model, we inferred that compound **5e**, at an oral dose of 5 mg/(kg day), increased the expression of osteogenic genes (RUNX2, BMP-2, Col1, and OCN) and the bone formation rate and significantly promoted bone regeneration at the fracture site, as evidenced by the increased bone volume/tissue fraction compared with vehicle-treated rats. Furthermore, structure−activity relationship studies and pharmacokinetic studies suggest **5e** as a potential bone anabolic lead for future osteoporosis drug development.

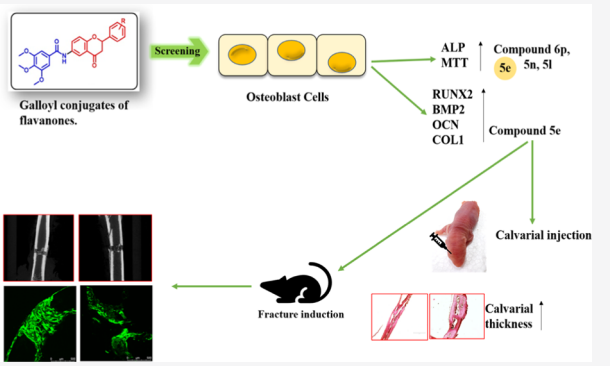

INTRODUCTION

Osteoporosis, a silent metabolic disorder, is depicted by an aberrant bone remodeling process. Remodeling of a living and dynamic tissue like bone is incessantly balanced by two opposite events, i.e., bone resorption and bone formation. Osteoclasts and osteoblasts are the two active participants of bone resorption and bone formation processes, respectively, and in bone remodeling, these two processes are tightly coupled.[1] An imbalance in the homeostasis of bone remodeling that causes greater bone resorption over bone formation results in osteoporosis, which is characterized by low bone mass and structurally compromised bone tissue, thereby predisposing bones to a high risk of fractures.[2] Osteoporosis is not only associated with compromised bone mechanical strength but also a decreased quality of life. According to recent studies, osteoporosis afflicts about 200 million globally and this number is expected to surge 2-fold by 2040.[3]

As of now, suppression of osteoclast functions and stimulation of osteoblast activity are the key therapeutic tools for rectifying the aberrant bone remodeling process in osteoporosis. Currently, drugs of two different categories are in clinical use, which include antiresorptive and bone anabolic agents. Antiresorptive agents, e.g., bisphosphonates (alendronic acid, ibandronic acid, risedronic acid, and zoledronic acid), selective estrogen receptor modulators (SERMs) like raloxifene, and monoclonal antibody against RANKL (denosumab), have an ameliorative effect in halting further bone resorption in osteoporosis patients. The chief pitfall with the use of antiresorptive agents is that the amount of bone that is already lost cannot be restored.[4] Bone morphogenetic proteins (BMPs), which belong to the transforming growth factor β (TGF-β) superfamily, have been reported to promote fracture healing in various animal models and in humans. At the fracture sites, BMPs are generally delivered as recombinant proteins (BMP-2/BMP-7). BMP-2 is expressed by the bone-forming osteoblast cells and promotes osteoblast differentiation and bone regeneration in various animal models.[5] Local application of BMP-2 at the fracture site has received FDA approval for orthopedic use. However, poor bioavailability, expensive synthesis, and purification process of recombinant BMP-2 protein limit its systemic use. Hence, in this direction, synthesis of small, orally efficacious, and inexpensive BMP-2 upregulators/secretagogues may provide new bone anabolic agents that

Received: January 21, 2021

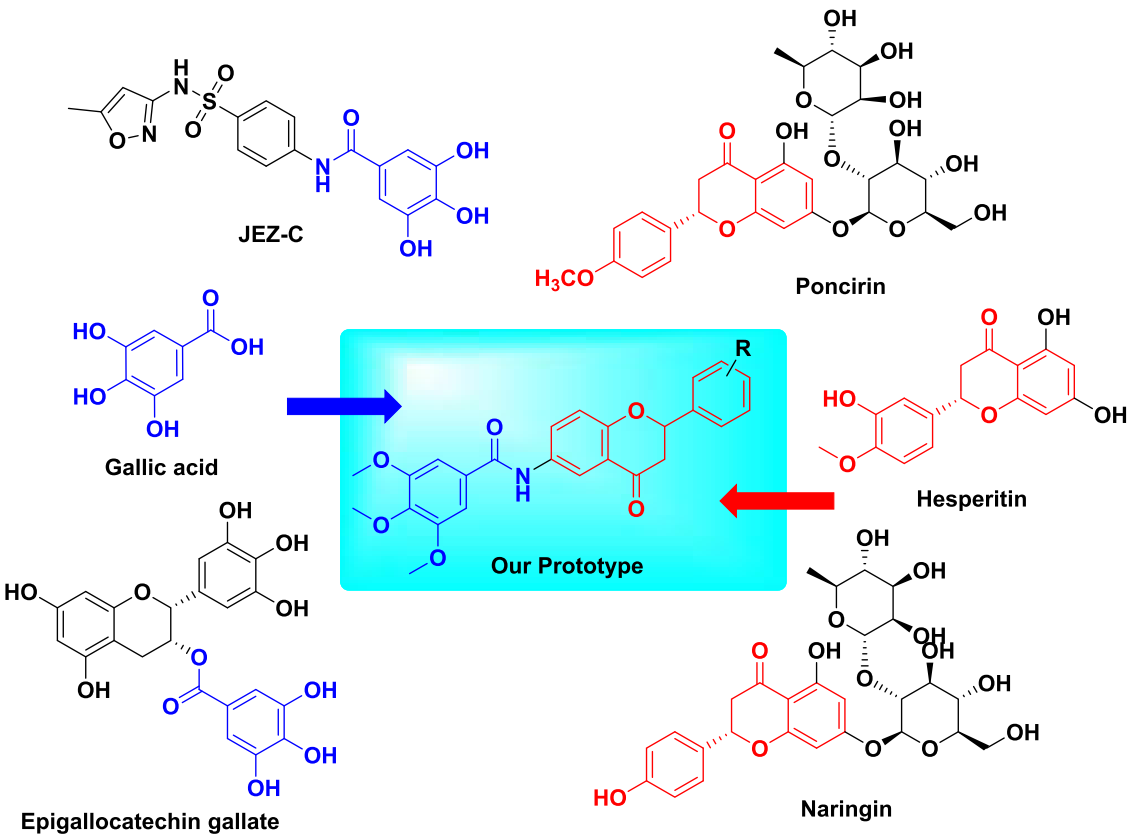

Figure 1. Molecular hybridization approach for designing galloyl conjugates of flavanones.

Scheme 1. Synthesis of Galloyl Conjugates of Flavanones[a]

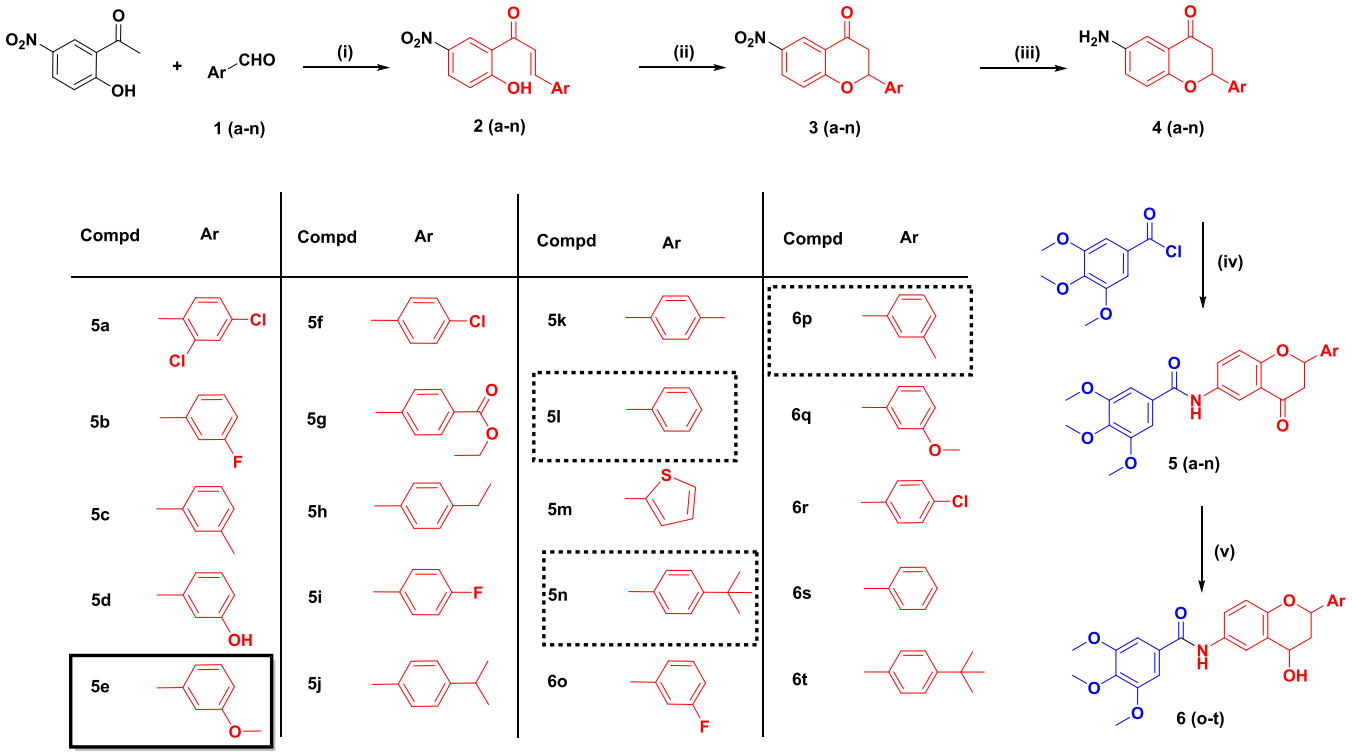

[a]Reagents and conditions: (i) NaOH (4 M), ethanol, r.t. (overnight); (ii) conc. H_2SO_4, ethanol, reflux (3−4 h); (iii) Fe, $CaCl_2$, H_2O, ethanol, reflux (3−4 h); (iv) Et_3N, dichloromethane (DCM), r.t.; (v) $NaBH_4$, r.t. 1 h.

https://doi.org/10.1021/acs.jmedchem.1c00112
J. Med. Chem. XXXX, XXX, XXX−XXX

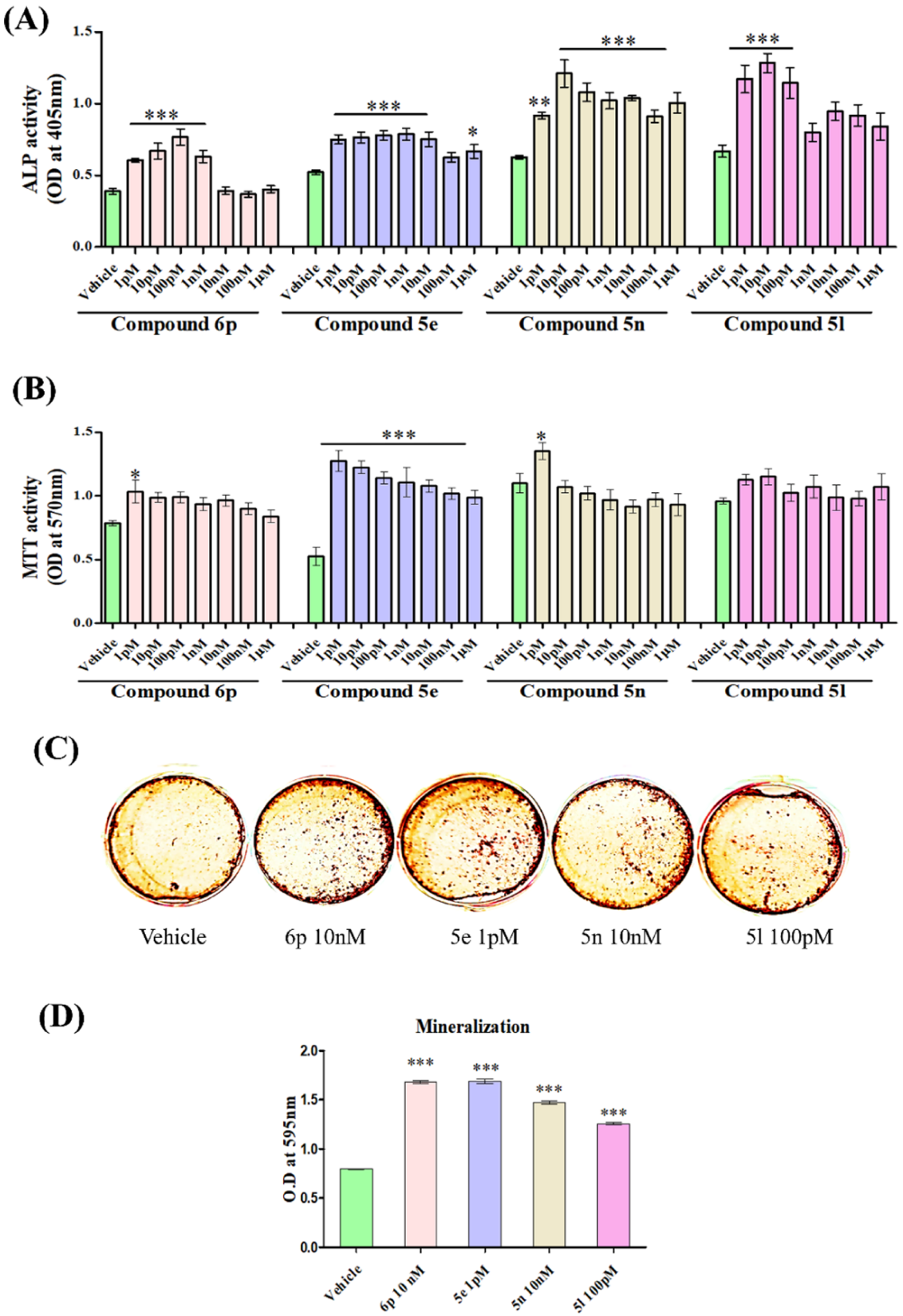

Figure 2. (A) Compounds stimulating osteoblast differentiation in an ALP activity assay. **6p**, **5e**, **5n**, and **5l** treatments showed elevated ALP production compared to the vehicle-treated cells. (B) Compounds stimulating cell viability. **6p**, **5e**, **5n**, and **5l** treatments enhanced the viability of osteoblasts compared to the vehicle-treated cells. (C) Compounds promoting mineralized nodule formation as assessed by Alizarin red-S staining shown by the representative microscopic images and (D) quantification of the extracted stain. Data are represented as mean ± standard error of the mean (SEM) of three independent experiments compared to the vehicle, $*p < 0.05$, $**p < 0.01$, and $***p < 0.001$ vs vehicle.

https://doi.org/10.1021/acs.jmedchem.1c00112
J. Med. Chem. XXXX, XXX, XXX−XXX

not only induce new bone formation but also show lesser adverse effects.[6]

Currently available bone anabolic agents including teriparatide, abaloparatide, and romosozumab are biologics and are administered through the parenteral route.[7,8] Treatment adherence is greater with oral medication over the parenteral drugs, and hence, oral bone anabolic drug is an unmet clinical need.

Gallic acid or 3,4,5-trihydroxy benzoic acid and its derivatives embrace a group of polyphenolic compounds belonging to the family of natural antioxidants. In nature, they are present in different forms such as methylated gallic acids (e.g., syringic acid), galloyl conjugates of catechin derivatives (e.g., epigallocatechin), and polygalloyl esters of glucose, quinnic acid, or glycerol. These polyphenolic compounds are known to possess strong antioxidant and anti-inflammatory activities.[9] Besides, gallic acid has been known for its osteogenic activity since long.[10] However, despite having substantial pharmacological responses, the hydrophilicity of gallic acid has hampered its implementation as a potent antioxidant clinically by lowering its absorption, increasing the rate of elimination, and decreasing its bioavailability. Also, a structure−activity relationship study carried out on gallic acid and its derivatives for evaluating their antioxidant ability revealed that derivatives with hydrophobicity higher than gallic acid such as epigallocatechin gallate and epicatechingallate have better scavenging effects in comparison to gallic acid.[11] Thus, to improve the bone anabolic potential of gallic acid, sulfonamide-based gallates such as JEZ-C and ZXHA-TC were synthesized, and indeed, both displayed promising bone anabolic agents.[12,13]

From the above description, it was reasonable to consider the synthesis of gallic acid to harness its salutary biological effects and improve on its major limitation such as poor bioavailability.[14] Moreover, several studies have been reported, in which flavanones demonstrated a wide spectrum of biological activities. Interestingly, flavanones such as Naringin,[15] Hesperetin,[16] and Poncirin[17] have been reported to possess an osteoprotective effect, and these reports prompted us to design, synthesize, and evaluate amide-based galloyl conjugates of flavanones, which have not been explored much to date for their skeletal action. Figure 1 shows the strategy for designing galloyl conjugates of flavanones.

RESULTS AND DISCUSSION

Chemistry. A general synthesis of galloyl conjugates of flavanones **5a−n** is outlined in Scheme 1. Their synthesis started with the condensation of 2′-hydroxy-5′-nitroacetophenone **1a−n** with the corresponding aromatic aldehyde in a basic medium, which afforded 2′-hydroxy-5′-nitro substituted chalcones **2a−n**.[18] These chalcones were then refluxed in ethanol in the presence of conc. H_2SO_4 to give 5′-nitro substituted flavanones **3a−n**.[19] Thus-obtained nitro flavanones were reduced with Fe/$CaCl_2$ in aqueous ethanol to corresponding amines **4a−n** and subsequently coupled with 3,4,5-trimethoxybenzoyl chloride to give the final galloyl conjugates of flavanones **5a−n** in good yields.[20] To study their structure−activity relationship (SAR), six flavanones were further reduced with $NaBH_4$ to obtain galloyl conjugates of flavan-4-ols **6o−t**.[21] All of the newly synthesized galloyl conjugates were characterized by ^{1}H NMR, ^{13}C NMR, two-dimensional (2D) NMR, and high-resolution mass spectrometry.

Characterization of Compound ***5e***. The presence of the characteristic peak of H-2 as a doublet of doublets at δ5.46 and the diastereotopic H-3a and H-3b protons as two doublet of doublets at δ2.89 and 3.07, respectively, in ^{1}H NMR spectra of the most active compound **5e** confirmed the presence of the chromane ring of the flavanone structure. H-3a and H-3b of the flavanone ring showed geminal coupling with a coupling constant of 17.0 Hz. On the other hand, a coupling constant value of 13.2 Hz for H-2 and H-3a indicated the axial position for H-3a, whereas $J_{2,3b}$ = 2.8 Hz further confirmed the equatorial position of H-3b.[18] In this way, the half chair conformation of the chromane ring in flavanone was confirmed. In addition, one singlet at δ 3.85 (s, 3H) corresponded to the methoxy group of flavanone, while two singlets at 3.90 (s, 3H) and 3.93 (s, 6H) corresponded to the three methoxy groups of gallic acid. Peaks ranging from δ 6.91 to 8.15 correspond to the remaining nine aromatic protons. ^{13}C NMR spectra also showed all of the relevant number of resonances corresponding to 26 carbon atoms. The characteristic peaks at δ 165.7 and 192.0 confirmed the presence of carbonyl of the amide bond through which gallic acid and flavanone were coupled and carbonyl of the flavanone structure, respectively. Furthermore, the molecular ion peak $[M + H]^+$ at m/z = 464.1705 in the high-resolution mass spectra (HRMS) established its molecular formula as $C_{26}H_{26}NO_7$. Based on the above spectral data evidence and reported literature values, compound **5e** was confirmed to be 3,4,5-trimethoxy-*N*-(2-(3-methoxyphenyl)-4-oxochroman-6-yl) benzamide. Further, it was observed that the stereocenter at the C-2 position imparts chirality to compound **5e** and thus was obtained as a racemic mixture; it was resolved into its component isomers with the use of chiral separation over normal-phase high-performance liquid chromatography (HPLC). Assignment of the absolute configuration *R*/*S* was achieved utilizing circular dichroism (CD) spectroscopy analysis.[22]

Biological Activity. *Primary Screening of Flavanones Using Osteoblast Differentiation Assay.* In calvarial osteoblast cells, alkaline phosphatase (ALP) activity, a surrogate of osteoblast differentiation, was used to screen the synthesized flavanones.[23] The ALP activity was read with a spectrophotometer, and the optical density was measured at 405 nm in calvarial osteoblast cells by treating them with test compounds at concentrations ranging from 1 pM to 1 μM. Four compounds, namely, **6p**, **5e**, **5n**, and **5l**, among the total of 20 exhibited increased ALP activity in comparison to the vehicle (with no treatment). Compound **6p** increased the ALP activity significantly at concentrations ranging from 1 pM to 1 nM, compound **5e** increased the activity from 1 pM to 10 nM, compound **5n** increased it at concentrations from 1 pM to 1 μM, and compound **5l** increased the activity at 1, 10, and 100 pM, as shown in Figure 2A. Table 1 shows the E_{max} values (maximum effective concentration) for all four bioactive compounds. This experiment evidently demonstrated that these four compounds act as promising osteoblast differentiating agents.

Table 1. EC_{max} of the Four Bioactive Compounds Determined by the ALP Assay

compound	**6p**	**5e**	**5n**	**5l**
EC_{max}	100 pM	1 nM	10 pM	10 pM

Enhanced Proliferation of Osteoblasts within Effective Concentrations. Four bioactive compounds were tested for toxicity on calvarial osteoblast cells by the cell viability assay using 3-(4,5-dimethylthiazol-2-yl)-2,5-diphenyltetrazolium bro-

https://doi.org/10.1021/acs.jmedchem.1c00112
J. Med. Chem. XXXX, XXX, XXX−XXX

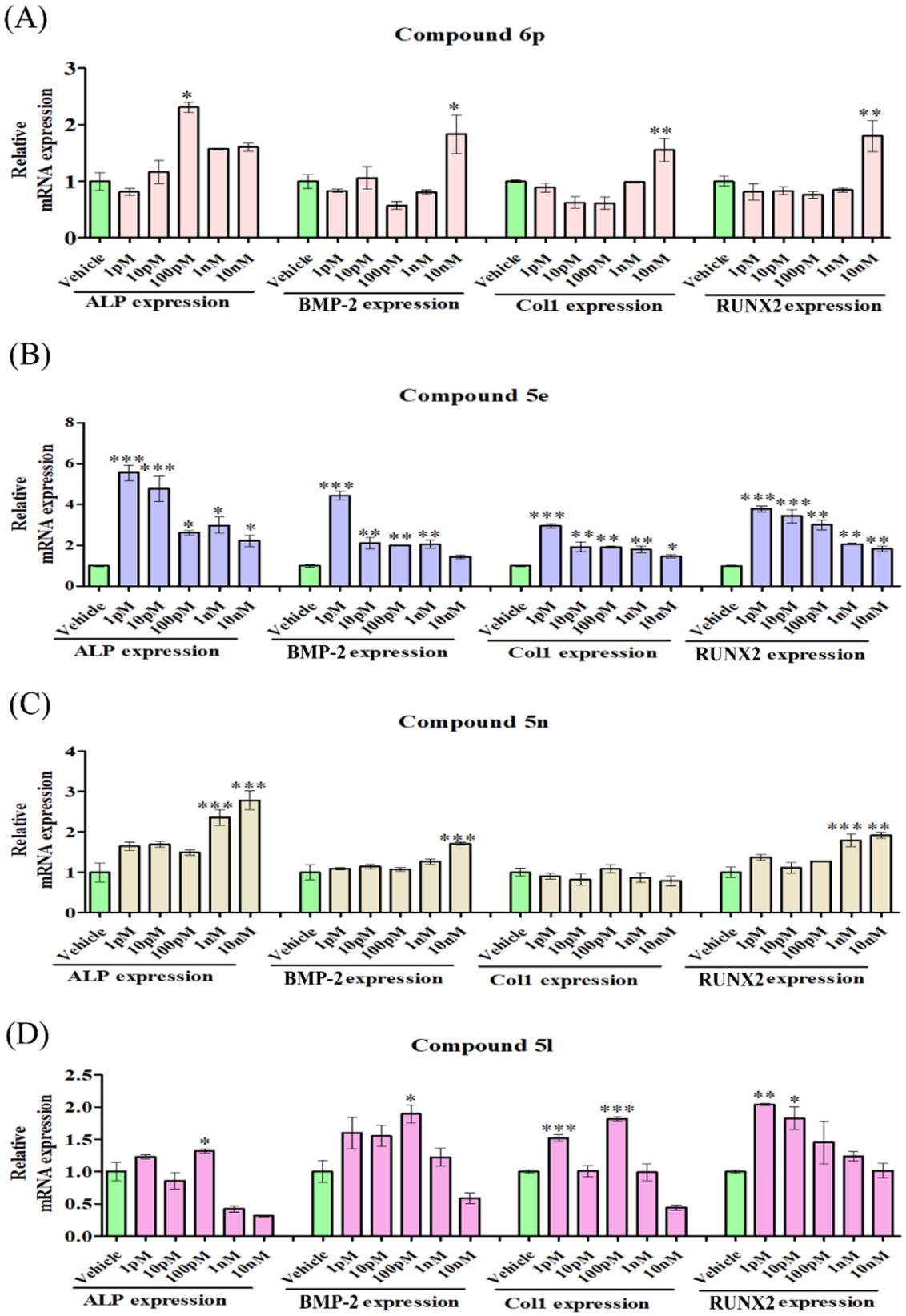

Figure 3. Assessment of osteogenic gene expression by qPCR. (A) **6p**, (B) **5e**, (C) **5n**, and (D) **5l** upregulate ALP, BMP-2, Col1, and RUNX2 expressions compared to the vehicle. Data are represented as mean ± SEM of three independent experiments relative to the vehicle, $*p < 0.05$, $**p < 0.01$, and $***p < 0.001$ vs the vehicle.

mide (MTT). Compounds **6p**, **5e**, **5n**, and **5l** showed no toxicity to osteoblast cells when compared with the vehicle group at concentrations ranging from 1 pM to 1 μM. Furthermore, compound **5e** increased proliferation (Figure 2B) at concen-

https://doi.org/10.1021/acs.jmedchem.1c00112
J. Med. Chem. XXXX, XXX, XXX−XXX

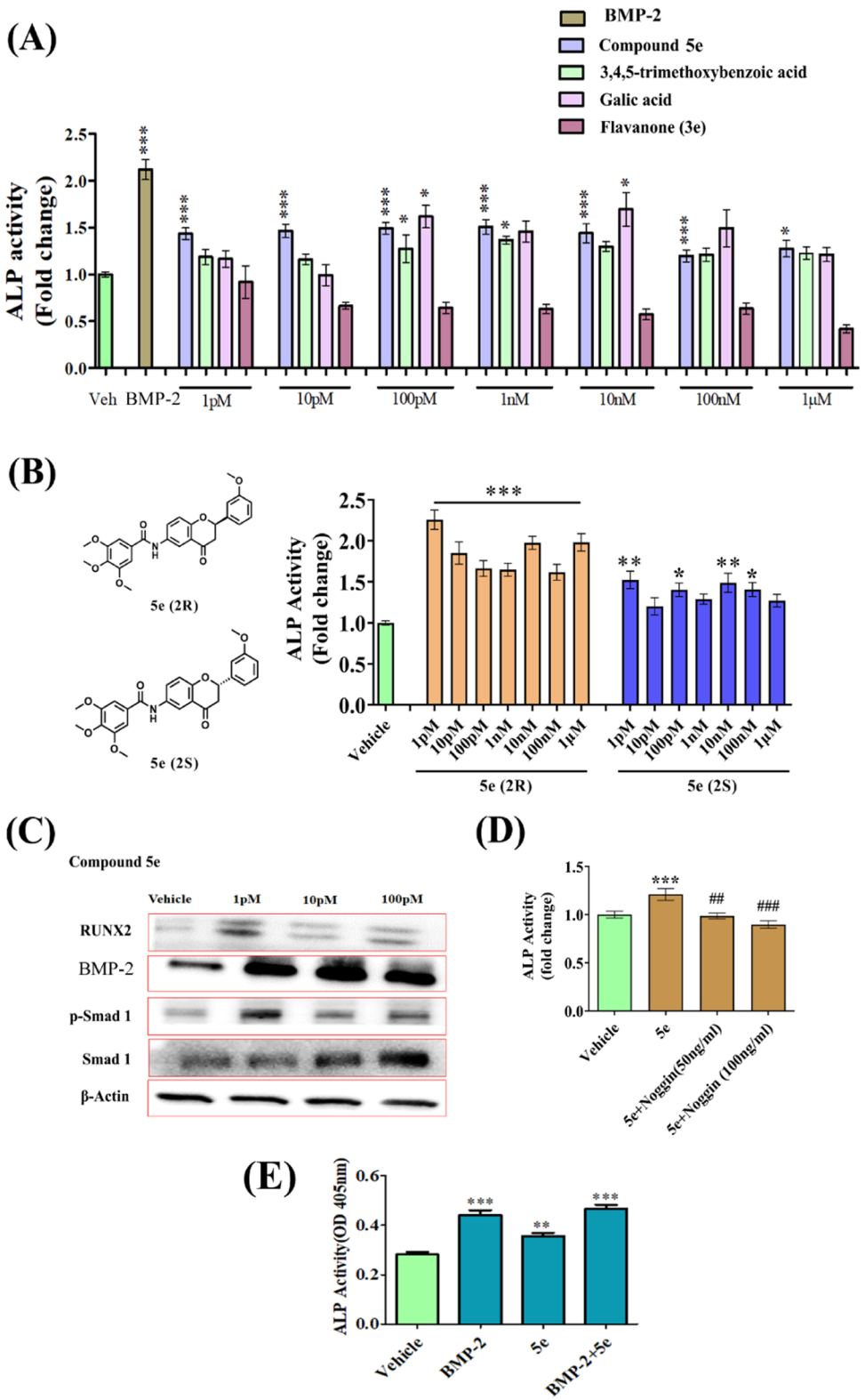

Figure 4. (A) **5e** showing elevated ALP activity at the indicated concentrations in rat primary osteoblast cells compared with its other structural analogues. (B) **5e** (2*R*) and **5e** (2*S*) exhibited elevated ALP activity at the indicated concentrations and compared with the vehicle-treated control. (C) **5e** differentiated osteoblast cells through the BMP-2/Smad pathway. Immunoblot showing elevated expressions of RUNX2, BMP-2, p-Smad 1, and Smad 1 at 1 pM. (D) **5e** increased the ALP activity in osteoblasts, and the effect was completely abrogated by noggin, a BMP-2 antagonist. (E) Presence of **5e** had no effect on the ALP activity of BMP-2 (100 ng/mL). Data are represented as mean ± SEM compared to the vehicle, $*p < 0.05$, $**p < 0.01$, and $***p < 0.001$ vs vehicle and $^{\#}$ **5e** vs Noggin.

https://doi.org/10.1021/acs.jmedchem.1c00112
J. Med. Chem. XXXX, XXX, XXX−XXX

trations ranging from 1 pM to 1 μM, whereas compounds **6p** and **5n** showed a significant increase in proliferation at 1 pM (Figure 2B).

Mineralization Ability in Calvarial Osteoblast Cells. Compounds selected from the series of 20 compounds after the assessment of bioactivity in the ALP assay were further analyzed for their mineralizing ability as it is a physiological process in the bone due to the inherent potential of osteoblasts to differentiate and form mineralized nodules *in vitro*.[24] Calvarial osteoblast cells were treated with different concentrations of compounds, and cultures were maintained for 14 days. Based on our ALP assay, we selected the lowest active dose of each compound and the mineralization assay was performed at the lowest active dose. Cells were fixed and stained with Alizarin red-S, a calcium chelator (Figure 2C).[25] Compounds **6p**, **5e**, **5n**, and **5l** showed significantly increased mineralized nodules compared to the untreated cells following the quantification of optical density of Alizarin red-S extraction from stained cultures (Figure 2D). These data suggested that **6p** and **5n** were the most potent at 10 nM, **5e** at 1 pM, and **5l** at 100 pM in inducing osteoblast mineralization *in vitro* (Figure 2D).

Active Compounds Increased the Gene Expression of Osteogenic Markers. After examining the mineralizing ability of active compounds, we studied their response on the expression of various osteogenic genes including RUNX2 (Runt-related transcription factor 2), BMP-2, ALP, and Col1 (Type 1 collagen) in calvarial osteoblast cells by the quantitative real-time polymerase chain reaction (qPCR). Housekeeping gene glyceraldehyde 3-phosphate dehydrogenase (GAPDH) was used as an internal control (to normalize input RNA). RUNX2, a bone-specific transcription factor, is a master transcription factor required for determination of osteoblast cell fate.[26] A number of transcriptional regulators interact with RUNX2 to control osteoblast differentiation. RUNX2 upregulates the expression of ALP and Col1 to drive osteoblast differentiation.[27]

BMP-2 is a strong inducer of bone formation and is under the regulation of the parathyroid hormone[28] and estrogen.[29] The mRNA levels of BMP-2, RUNX2, ALP, and Col1 were quantified by qPCR after the treatment of calvarial osteoblasts with bioactive compounds at concentrations ranging from 1 pM to 10 nM. **6p** increased the expressions of ALP, BMP-2, Col1, and RUNX2 by 2.3-, 1.83-, 1.55-, and 1.80-fold, respectively, at 100 pM for ALP and others at 10 nM concentrations (Figure 3A).

5e increased the expression of these osteogenic genes at a wide range of concentrations, but at its minimum active concentration, i.e., 1 pM, the expressions of ALP, BMP-2, Col1, and RUNX2 were increased by 5.5-, 4.4-, 2.9-, and 3.7-fold, respectively (Figure 3B). **5n** increased ALP, BMP-2, and RUNX2 expressions by 2.8-, 1.7-, and 1.9-fold, respectively; however, it did not significantly increase the expression of Col1 (Figure 3C). **5l** increased the expressions of ALP, BMP-2, and Col1 by 1.3-, 1.9-, and 1.8-fold at 100 pM and RUNX2 by 2-fold at 1 pM (Figure 3D). From this experiment, we confirmed the osteogenic effect of four compounds. To determine the lead compound, we considered the lowest active *in vitro* osteogenic concentration and the highest fold induction of the expression of osteogenic genes by these four compounds. Compound **5e** best met these two criteria.

*Comparison of **5e** with Other Structural Analogues.* The osteoblastic ALP activity of **5e** was compared with 3,4,5-trimethoxybenzoic acid, gallic acid, and flavanone **3e**. Cells treated with BMP-2 were taken as a positive control. **5e** significantly increased the ALP activity at 1 pM, whereas the other three required concentrations higher than this (Figure 4A). **5e** increased the ALP activity compared to 3,4,5-trimethoxybenzoic acid ($p < 0.05$), gallic acid ($p < 0.05$), and flavanone **3e** ($p < 0.01$). At 10 pM, **5e** showed a greater activity compared with 3,4,5-trimethoxybenzoic acid ($p < 0.05$), gallic acid ($p < 0.01$), and flavanone **3e** ($p < 0.001$). At 100 pM, the same pattern was also observed although not significant. For the statistical examination, a two-tailed Student's t test was employed.

To confirm the activity of the racemic mixture of the lead compound **5e**, isomers were separated and both (2*R* and 2*S*) were found active compared to the vehicle, as indicated by the enhanced ALP activity (Figure 4B). This data suggested that the activity of **5e** as a racemic mixture was not dependent on any one isomer. Changes in the protein level of osteogenic target genes were quantified with reference to β-actin. Calvarial osteoblasts were treated with **5e** (1, 10, and 100 pM) for 48 h, which resulted in an increase in RUNX2 and BMP-2 expressions maximally at 1 pM as assessed by immunoblotting (Figure 4C). Moreover, phosphorylation of Smad 1 (p-Smad 1), the downstream of BMP receptor activation, was strongly increased by **5e**, which suggested that BMP-2 upregulation by the compound likely elicited the BMP receptor response triggering osteogenesis (Figure 4C).[30]

Next, we studied whether or not the osteogenic effect of **5e** was BMP-2 dependent. Noggin is an endogenous BMP antagonist and is known to diminish osteoblast differentiation,[28] thereby regulating the amount of bone deposition at the physiologic level. The presence of noggin completely abrogated the osteogenic effect of **5e**, as assessed by ALP production from osteoblasts (Figure 4D), thus suggesting that **5e** required BMP-2 to achieve an osteogenic impact. Furthermore, the osteogenic effect of BMP-2 was not altered by **5e**, thus suggesting that the compound signaled via the BMP-2 pathway (Figure 4E). Taken together, it appears that in osteoblasts, **5e** is a BMP-2 "secretagogue".

Because BMP-2 is endogenously produced by osteoblasts and acts locally to promote bone formation, we considered it important to assess whether **5e** interfered with the action of BMP-2. At the functional level, two BMP-2 molecules form an intermolecular disulfide bond (Cys78 from both ligand molecules).[30] We performed molecular docking to predict the binding of **5e** with the BMP-2 dimer and to test whether it affected the dimer (Supporting Figures S3 and S4). Indeed, the prediction supports the preservation of the BMP-2 dimer and further received credence from Figure 4E showing that BMP-2 function is completely retained in the presence of **5e** besides proving that **5e** exclusively signals through the BMP-2-dependent mechanism involving its upregulation.

*In Vivo Evaluation of **5e** as an Osteoanabolic Agent.* To provide *in vivo* evidence of the osteogenic effect of **5e**, we administered it subcutaneously in 7 day old rat pups for 6 days at 1 mg/kg, 5 mg/kg, and 10 mg/kg doses. Once the treatment was over, pups were sacrificed and the calvarial tissue was isolated for each pup to measure the mRNA expression of osteogenic genes including BMP-2, RUNX2, Col1, and osteocalcin (OCN). We also analyzed the quantitative histomorphometry and histology in response to **5e** treatment. Neonatal calvaria is rich in preosteoblasts, and we used newborn rat pups in a subchronic dosing model to assess rapid osteogenic response if any achieved by the stimulation of intramembranous ossification of a test

https://doi.org/10.1021/acs.jmedchem.1c00112
J. Med. Chem. XXXX, XXX, XXX−XXX

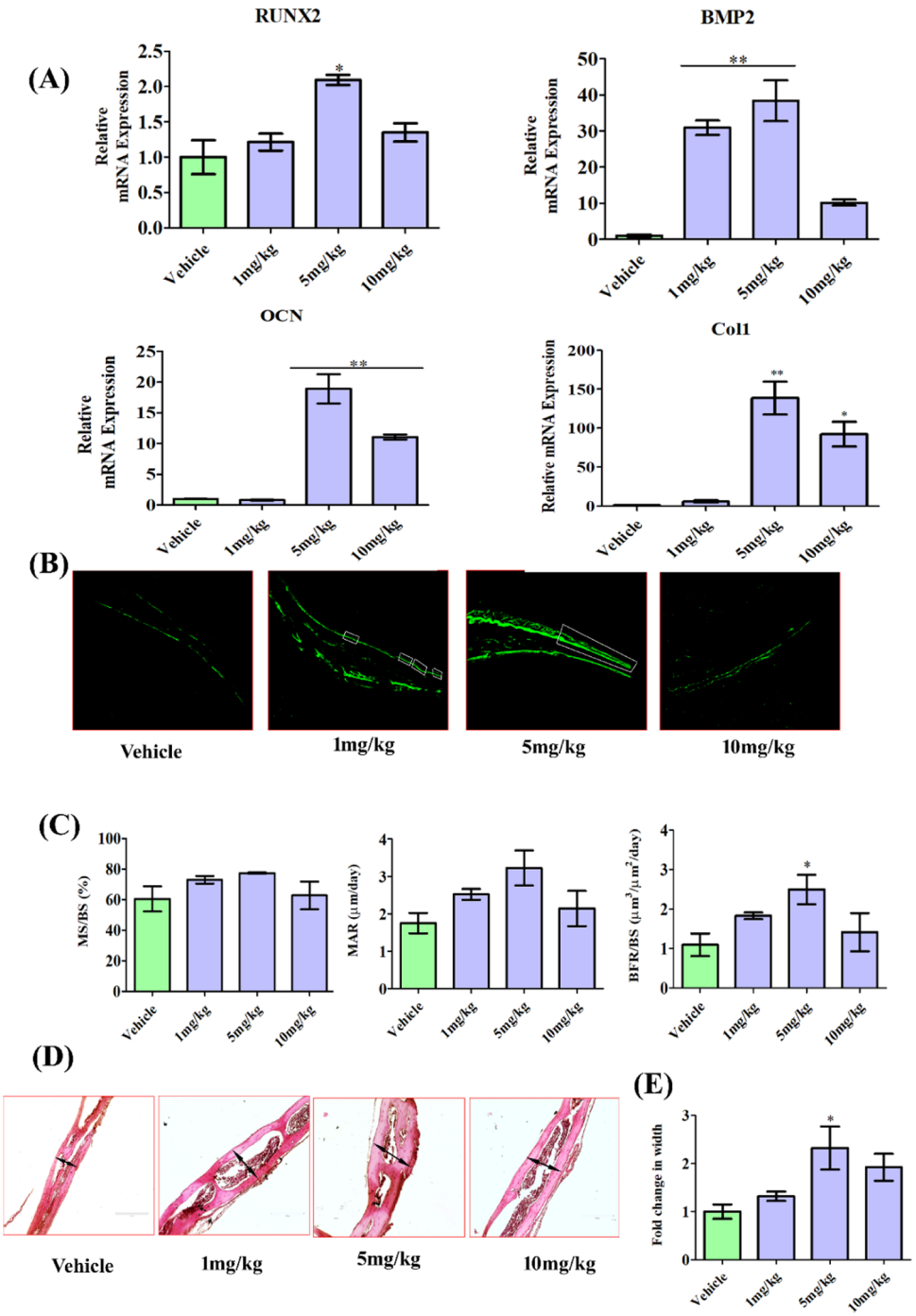

Figure 5. (A) **5e** upregulated mRNA expressions of RUNX2, BMP-2, OCN, and Col1 in the calvarial tissue. (B) **5e** induced *in vivo* bone formation measured by double calcein labeling and shown are the representative images. (C) Quantification of various parameters derived from the double labeling experiment at the indicated doses; MS/BS, mineralizing surface normalized with bone surface; MAR, mineral apposition rate; and BFR, bone formation rate. Box indicates continuous double labeling at 5 mg/kg dose and discontinuous double labeling at 1 mg/kg dose. (D) Representative histological sections of the calvarial tissue showing increased width at the indicated doses compared with the vehicle and as indicated by the bidirectional arrow. (E) Quantification of the data derived from panel D. Data are represented as mean ± SEM compared to the vehicle, $*p < 0.05$ and $**p < 0.01$ vs the vehicle.

compound *in vivo*[31,32] before undertaking confirmatory tests in models that require a prolonged dosing regimen.

All osteogenic genes in the calvaria were maximally stimulated by **5e** at 5 mg/kg dose (Figure 5A). RUNX2 was upregulated by ∼2-fold ($*p < 0.01$) at 5 mg/kg dose compared with the vehicle. BMP-2 expression showed a robust dose-dependent increases in response to **5e** between 1 and 5 mg/kg doses, and the induction ranged from 30- to 38-fold over the vehicle-treated cells. Expression of the most abundant bone matrix protein, Col1, was increased by ∼138- and ∼92-fold by 5- and 10 mg/kg doses, respectively. Expression of OCN, the most abundant non-collagenous protein of the matrix, was upregulated by ∼18-fold and ∼10-fold, respectively, by 5 and 10 mg/kg doses and notably displayed a dose-dependent decrease. OCN upon carboxylation favors calcium nucleation, a crucial step in mineralization.[33] Therefore, our *in vitro* and *in vivo* data suggest that **5e** exerts its

https://doi.org/10.1021/acs.jmedchem.1c00112
J. Med. Chem. XXXX, XXX, XXX−XXX

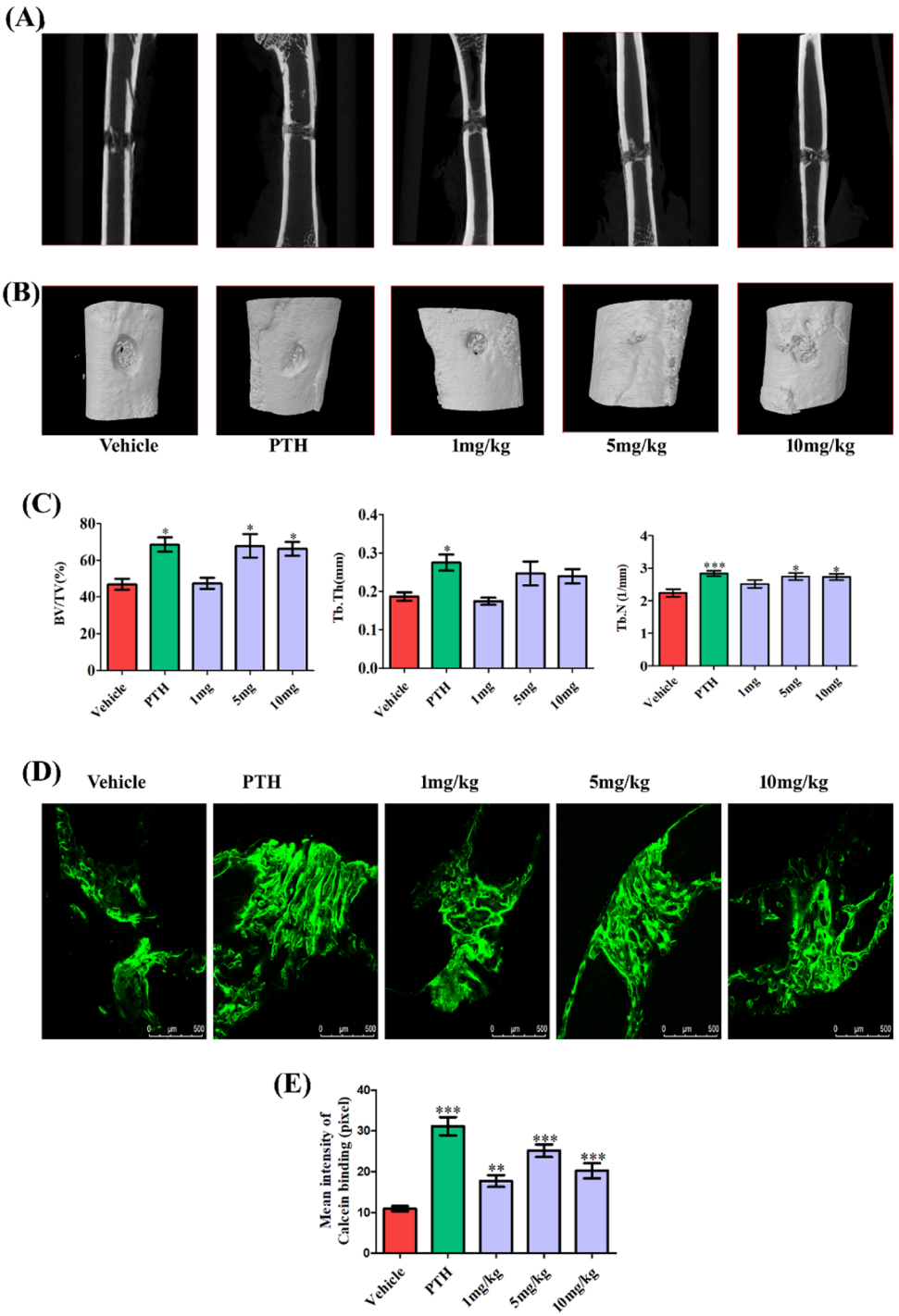

Figure 6. **5e** promotes fracture healing. (A) Representative 2D structure of the fracture site from microCT. (B) 3D representations of the same. (C) **5e** at 5 mg/kg dose shows an increased bone volume/tissue volume fraction (BV/TV %), trabecular thickness (Tb.Th.), and trabecular number (Tb.N) of callus compared to the vehicle. (D) Representative microscopic images of calcein labeled callus (deposition of nascent bone) at the fracture site. (E) Mean intensity of calcein binding quantified from the images shown in panel (D). Data are represented as mean ± SEM compared to the vehicle, $*p < 0.05$, $**p < 0.01$, and $***p < 0.001$ compared with the vehicle.

osteogenic effect by increasing the synthesis of the matrix protein Col1 and mineralization by increasing OCN.

5e *Promotes New Bone Formation in Calvaria.* We analyzed surface referent bone formation that serves as the "litmus" test for osteoanabolic effect.[34] Time-spaced calcein labeling (Figure 5B) was used to calculate various parameters shown in Figure 5C. The mineral apposition rate (MAR), a measure of osteoblast vigor, showed an increasing trend at 5 mg/kg dose of **5e** but did not reach significance. The bone formation rate (BFR), a cumulative measure of mineralized bone formation per unit time, however, was significantly increased at 5 mg/kg dose over the vehicle ($*p < 0.01$) (Figure 5B). The bone formation rate in 10 mg/kg is greater than or equal to the vehicle group.[35]

5e *Increases Calvarial Thickness In Vivo.* We next assessed whether or not an increase in BFR translated to calvarial

https://doi.org/10.1021/acs.jmedchem.1c00112
J. Med. Chem. XXXX, XXX, XXX−XXX

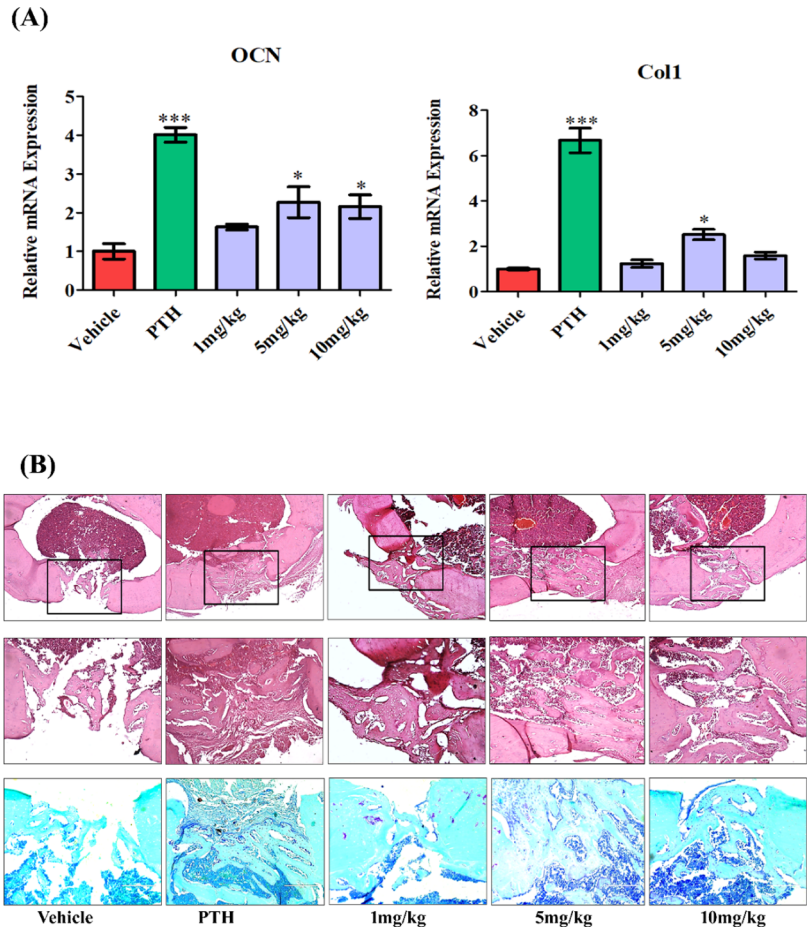

Figure 7. (A) Gene expressions of OCN and Col1 at the newly formed callus. (B) Histological representation of the fracture site and associated callus as seen in H&E staining and toluidine blue staining. The first panel indicates the lower magnification of 4×, whereas the other two panels indicate the higher magnification (10×) of the callus region. Data are represented as mean ± SEM compared to the vehicle, $*p < 0.05$ and $***p < 0.001$ vs the vehicle.

thickness by quantitative histology. Hematoxylin and eosin staining of the sections showed an increase in calvarial thickness induced by **5e** at the 5 mg/kg dose over the vehicle ($*p < 0.01$) (Figure 5D,E).[35]

*Evaluation of **5e** in Fracture Healing through Micro-computed Tomography (μCT) and Bone Histomorphometry.* Having shown that **5e** has an osteogenic effect in neonatal animals characterized by heightened bone formation, we next assessed whether or not it has an osteogenic effect in adult animals. To this aim, we tested its bone regenerative ability in a femur osteotomy (fracture) model, which represents a stable fracture that heals by primary ossification.[36] The treatment of compound **5e** was started the very next day of the injury and was given once daily for 14 days at doses of 1, 5, and 10 mg/kg body weight, orally. Human parathyroid hormone (1−34) (PTH) was used as the comparator as it is the most widely used standard-of-care osteogenic drug and is reported to mediate its effect through BMP-2.[28] Moreover, BMP-2 has no permissible systemic use. In comparison to the vehicle, **5e** healed the fracture and promoted callus formation at the injury site as shown by 2D and three-dimensional (3D) representations of μCT (Figure 6A,B). μCT analysis showed that at 5 mg/kg dose, **5e** increased BV/TV by ∼44.3% at 5 mg/kg, which was comparable to PTH, which increased it by ∼46.0% when compared to the vehicle group. Tb.N was significantly increased, while Tb.Th showed an increasing trend in **5e**-treated rats compared with the vehicle (Figure 6C). Increased BV/TV, Tb.Th, and Tb.N at the fracture site indicated greater callus formation through new bone regeneration (woven bone), which would facilitate its transformation into the lamellar bone and improved callus biomechanical property.[37] From the calcein labeling study, we observed that **5e** (5 mg/kg) was comparable to PTH (130% increase with **5e** vs 184% with PTH) (Figure 6D,E). These data support drawing the conclusion that **5e** promotes fracture healing maximally at 5 mg/kg dose and the effect is comparable to the clinically used osteoanabolic drug PTH. PTH, due to its osteoanabolic properties, is suitable for fracture healing and has been reported in various studies and thus taken as a positive control. Its effectiveness and safety are also well established.[38,39]

***5e** Upregulated the Expressions of Col1 and OCN in Fracture Calluses.* Consistent with our observation with calvaria (Figure 5A), the expressions of OCN and Col1 too were upregulated by **5e** at the callus compared to the vehicle-treated animals. The fold increases of Col1 and OCN by **5e** were ∼2.5- and ∼2.2-fold, respectively (Figure 7A). Col1 is the most abundant matrix protein, and OCN is the most abundant noncollagenous protein, and together they provide the substrate and catalyze mineralization of the matrix. Upregulation of Col1 and OCN thus provides a mechanistic basis for increased calcein deposition (a surrogate of nascent bone formation) at the callus by **5e**.[40,41]

https://doi.org/10.1021/acs.jmedchem.1c00112
J. Med. Chem. XXXX, XXX, XXX−XXX

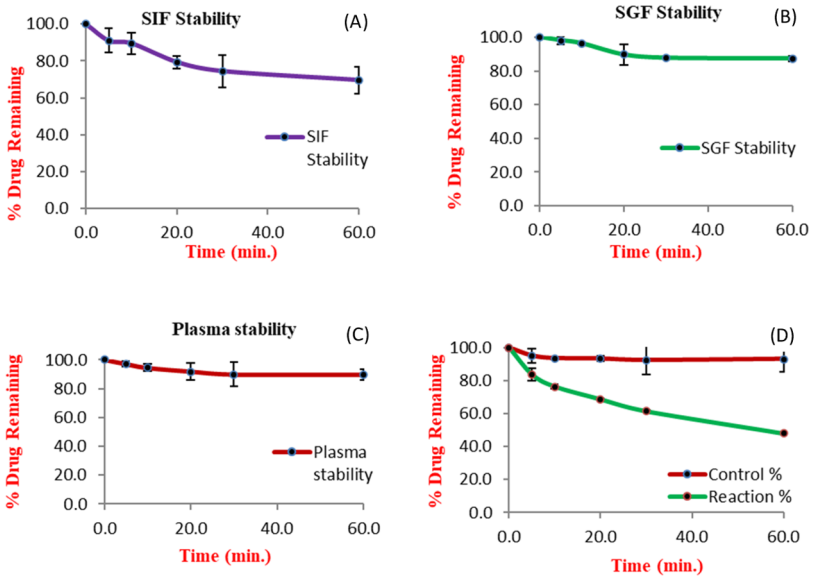

Figure 8. *In vitro* stability of compound **5e** in (A) simulated gastric fluid, (B) intestinal fluid, (C) plasma, and (D) rat liver microsomes (RLMs).

Effect of **5e** *on the Restoration of Bone Morphology.* Sections made through the calluses were stained with H&E and toluidine blue to determine the morphology and cartilage formation after **5e** and PTH treatments in adult rats. The connective tissue at the drill-hole site was replaced by the mature osteoblasts and fibrous callus in the **5e** (1, 5, and 10 mg/(kg day)) and PTH groups but not in the vehicle group. In the regions of the drill hole that are away from the periosteal and endosteal surfaces, the progenitor cells differentiate into chondrocytes and healing begins through endochondral ossification. Toluidine blue stains proteoglycan, a major cartilage protein, and accordingly, we observed extensive blue-stained areas in the sections from animals treated with **5e** (5 and 10 mg/kg) and PTH in contrast to sparse staining in the vehicle group (Figure 7B). Together with Figure 6D showing increased mineralization, enhanced proteoglycan formation by **5e** indicates stimulation of chondrogenesis besides the induction of osteogenesis.[42]

Overall, the effect of **5e** (5 mg/kg) on fracture healing and bone regeneration was comparable to that of PTH. As there is neither an oral osteoanabolic drug nor a small molecule (all three clinically used osteoanabolic drugs are biologics), the oral efficacy of **5e** on par with PTH is sufficiently tantalizing to ascribe it as a potential first-in-class oral osteoanabolic lead.

Metabolic Stability and Pharmacokinetic Studies. *In Vitro Stability Study in Gastric Fluid and Intestinal Fluid.* The stability of **5e** in simulated gastric fluid (SGF, pH 1.2) and simulated intestinal fluid (SIF, pH 6.5) is a prerequisite criterion for oral bioavailability. The result shows that the compound was stable in SIF (69.0 ± 5.01% remaining) and completely stable in SGF (88.0 ± 1.72% remaining) after 1 h of incubation at 37 °C, as shown in Figure 8A,B.

In Vitro Plasma and Microsomal Stability. Plasma stability of the compound is shown in Figure 8C, from which it can be concluded that **5e** was stable in rat plasma as 89.01 ± 3.74% remained intact in the plasma after 1 h of incubation. The *in vitro* microsomal stability assay was useful in measuring the intrinsic clearance Cl_{int} or in identifying the metabolites of compounds formed by liver enzymes. The compound was found to be stable without NADPH in rat liver microsomes (RLMs), as shown in Figure 8D. This revealed that **5e** was mainly metabolized by CYP enzymes, as 53% was metabolized after 1 h of incubation by RLM. The *in vitro* half-life ($t_{1/2}$) and Cl_{int} of the compound were calculated by plotting the normal logarithmic of the compound remaining over the incubation time up to 60 min. The half-life and Cl_{int} were found to be 62.02 h and 0.04 mL/min/mg, respectively. The significant RLM stability of **5e** could be attributed to the presence of the methoxy group that likely resisted hepatic glucuronidation observed in unmethylated flavonoids, resulting in the poor metabolic stability of the latter.[43]

In Vivo Pharmacokinetic Analysis. Gallic acid and flavonoids including flavanones suffer from poor oral bioavailability, which dampens their development as drugs despite displaying salutary effects *in vitro*. We therefore assessed the oral bioavailability of **5e** in adult rats. Figure 9 shows the mean plasma concentration

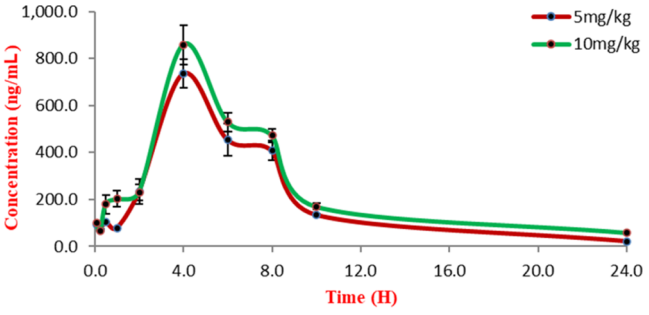

Figure 9. Mean plasma concentration vs time of **5e** at the indicated doses in adult male SD rats.

versus time profile in male Sprague-Dawley (SD) rats, and Table 2 shows the pharmacokinetic parameters that were estimated by Phoenix WinNonlin (version 8.1, CertaraInc). After the oral administration of **5e** (5 and 10 mg/kg), the maximum plasma concentration (C_{max}) and the overall systemic exposure (AUC) were found to be 736 (ng/mL) and 4824.5 (h*ng/mL), respectively, which shows the rapid absorption of the compound from the gut. Volume of distribution (V_d) and clearance (Cl) were found to be 8.42 (L/kg) and 1.04 (L/(h kg)), respectively. At 5 mg/kg (the most active dose), C_{max} of **5e** (736 ng/mL or 1.6

https://doi.org/10.1021/acs.jmedchem.1c00112
J. Med. Chem. XXXX, XXX, XXX−XXX

Table 2. Oral Pharmacokinetic Parameters of 5e

PK parameters	unit	dose 5 mg/kg	dose 10 mg/kg
C_{max}	(ng/mL)	736.00	857.50
AUC	(H*ng/mL)	4824.50	6531.55
$T_{1/2}$	H	5.60	5.85
Cl	L/(h kg)	1.04	1.54
V_d	L/kg	8.42	12.99
MRT	H	7.68	9.17

μM) was a log scale higher than its *in vitro* osteogenic EC_{max} of 1 nM, which suggested that the compound has substantial oral bioavailability.

The times taken for the systemic level to reduce to half (half-life, $t_{1/2}$) mean resident time (MRT) were found to be 5.6 (h) and 7.18 (h). It could be inferred from the above pharmacokinetic parameters that **5e** has an adaptable oral exposure and can therefore be considered a lead molecule for potential optimizations.

Structure–Activity Relationship (SAR). Primarily, all of the synthesized hybrids and their analogues were evaluated *in vitro* for their antiosteoporotic potential using the ALP activity, which yielded four active compounds **6p**, **5e**, **5n**, and **5l**. SAR deduced from the *in vitro* activity revealed that the phenyl ring of flavanone whether unsubstituted or with the substituent *p*-*tert*-butyl or *m*-methoxy group retained good activity. Interestingly, replacement of the phenyl ring with the heteroaromatic ring (**5m**) did not improve the activity, nor did the reduction of the carbonyl group (as in compounds **6o–t**). To show the indispensable role of pharmacophoric subunits in the overall activity of our hybrid molecule, a comparison of the osteoblastic ALP activity of **5e** with 3,4,5-trimethoxybenzoic acid, gallic acid, and flavanone (**3e**) was done, which revealed that although gallic acid and flavanones were active individually, their hybrid with a suitable substitution on the phenyl ring possessed better activity (Figure 4A). In addition, as **5e** turned out to be the most active in the series, further probing of its two isomers (2*R* and 2*S*) was done. Interestingly, both were found active and comparable to their racemic form **5e** (Figure 4B). Thus, chirality did not play any significant role in the bioactivity. Overall, it was inferred that both gallic acid and flavanone subunits constitute the core pharmacophore of the synthesized hybrids, with *p*-tert-butyl or *m*-methoxy substituents in the "C" ring of flavanone imparting the optimum levels of lipophilicity. A pictorial representation of the preliminary structure–activity relationships (SARs) is depicted in Figure 10.

CONCLUSIONS

A series of 20 new galloyl conjugates of flavanones were synthesized and studied in rat primary osteoblasts *in vitro* and in a drill-hole fracture model in rats for assessing their osteogenic potential. Through a series of *in vitro* and *in vivo* studies, we identified a lead compound **5e** that was orally bioavailable and induced osteoanabolic effect that was on par with the standard-of-care, PTH. At the mechanistic levels, **5e** induced osteogenic effect by acting as a BMP-2 secretagogue, i.e., by stimulating the synthesis of BMP-2 in osteoblasts. Given that an oral osteoanabolic drug is an unmet clinical need, **5e** appears suitable for further development as a novel class of osteoanabolic drug.

EXPERIMENTAL SECTION

General Chemistry. Reagents obtained from commercial sources were used without further purification. A 100–200-mesh silica gel was used in column chromatography for purification of compounds. The pace of chemical reactions was monitored by thin-layer chromatography (TLC) (silica gel plates with fluorescence F254). Melting points were uncorrected. The ^{1}H and ^{13}C NMR spectra were recorded at 400 and 100 MHz, respectively, using $CDCl_3$ and DMSO-d_6 as solvents. All chemical shift values were described in ppm and their multiplicities expressed as follows: m, multiplet; q, quartet; t, triplet; dd, double doublet; brd, broad doublet; d, doublet; brs, broad singlet; and s, singlet. The ESI-MS spectra were recorded on an ion trap LCQ Advantage Max mass spectrometer (Thermo Electron Corporation), and HRMS spectra were recorded by Q-TOF (Agilent 6520). All of the final compounds were found to be >95% pure as determined by an Agilent HPLC equipped with an Eclipse Plus C18 column (4.6 mm × 250 mm, 5 μm mesh size), with acetonitrile (solvent A) and water (solvent B) as an eluent in the ratio 9:1, at a flow rate of 0.80 mL/min and run time of 10 min. Detection was done by UV at 220 and 254 nm.

*General Synthesis of 2′-Hydroxy-5′-nitro Substituted Chalcones (**2a–n**).* To a well-stirred solution of 2′-hydroxy-5′-nitroacetophenone (10 mmol) and the respective aldehyde (10 mmol) in ethanol, sodium hydroxide (4 M) was added, and the reaction mixture was allowed to stir overnight at room temperature. On completion of the reaction, the reaction mixture was neutralized with dil. HCl (1 N) to precipitate chalcones, followed by filtration and drying in a vacuum. In any case,

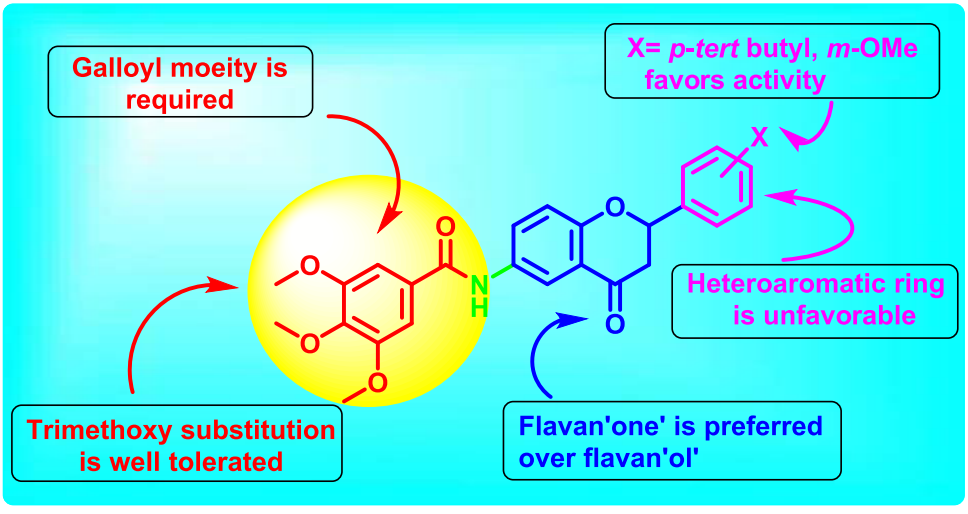

Figure 10. Structure–activity relationship (SAR) of synthesized compounds.

https://doi.org/10.1021/acs.jmedchem.1c00112
J. Med. Chem. XXXX, XXX, XXX–XXX

chalcone was not precipitated; it was extracted with ethylacetate, dried over anhyd. Na_2SO_4, and evaporated in a high vacuum.

*(E)-1-(2-Hydroxy-5-nitrophenyl)-3-(3-methoxyphenyl)prop-2-en-1-one (**2e**).* Yellow solid; yield: 80%; mp: 119−121 °C; ^{1}H NMR (DMSO-d_6, 400 MHz): δ3.81 (s, 3H), 7.04−7.07 (m, 1H), 7.19 (d, J = 9.1 Hz, 1H), 7.38 (t, J = 8.0 Hz, 1H), 7.43−7.45 (m, 2H), 7.74 (d, J = 15.8 Hz, 1H), 7.85 (d, J = 15.8 Hz, 1H), 8.34 (dd, J = 2.9 Hz, 9.2 Hz, 1H), 8.70 (d, J = 2.8 Hz, 1H), 12.67 (s, 1H); ^{13}C NMR (DMSO-d_6, 400 MHz): δ55.3, 114.0, 117.0, 118.4, 121.6, 123.3, 123.9, 126.6, 129.6 130.0, 135.7, 139.6, 145.1, 159.6, 164.6, 191.5.

*General Synthesis of 5′-Nitro Flavanones (**3a−n**).* The respective chalcones (0.01 mol) were suspended in ethanol followed by slow addition of concentrated H_2SO_4. The resultant reaction mixture was allowed to reflux for 4−6 h. On completion, the reaction mixture was allowed to cool down to room temperature followed by neutralization with saturated sodium bicarbonate solution and then extraction with ethylacetate. The combined organic layer was dried over anhyd. Na_2SO_4 and evaporated in a high vacuum. Thus-obtained 5′-nitro flavanones were pure enough to be directly used in the next step for reduction without any further purification by column chromatography.

*2-(3-Methoxyphenyl)-6-nitro-4H-chromen-4-one (**3e**).* Light-brown solid; yield: 74%; mp: 142−144 °C; ^{1}H NMR (DMSO-d_6, 400 MHz): δ2.99 (dd, J = 3.0 Hz, 17.0 Hz, 1H), 3.43 (dd, J = 12.8 Hz, 16.9 Hz, 1H), 3.78 (s, 3H), 5.86 (dd, J = 3.0 Hz, 12.8 Hz, 1H), 6.97−7.00 (m, 1H), 7.11−7.14 (m, 2H), 7.35−7.39 (m, 2H), 8.41 (dd, J = 3.0 Hz, 9.2 Hz, 1H), 8.52 (d, J = 2.8 Hz, 1H); ^{13}C NMR (DMSO-d_6, 400 MHz): δ42.7, 55.2, 79.6, 112.4, 114.3, 118.8, 119.9, 120.2, 122.2, 129.8, 130.5, 139.4, 141.5, 159.4, 165.1, 190.2.

*General Synthesis of 5′-Amino Flavanones (**4a−n**).* The above-obtained respective flavanones (0.01 mol) were subjected to reduction by suspending them in a mixture of ethanol and water, followed by addition of Fe powder (0.03 mol) and calcium chloride (0.01 mol). The resulting suspension was then refluxed for 4−5 h. On completion of the reaction, the reaction mixture was then filtered over celite for removal of iron residues followed by extraction with ethylacetate to obtain the respective amines.

*6-Amino-2-(3-methoxyphenyl)-4H-chromen-4-one (**4e**).* Reddish oil; yield: 89%; ^{1}H NMR (DMSO-d_6, 400 MHz): 2.72 (dd, J = 2.9 Hz, 16.9 Hz, 1H), 3.12 (dd, J = 12.9 Hz, 16.9 Hz, 1H), 2.78 (s, 3H), 4.98 (s, 2H), 5.46 (dd, J = 2.8 Hz, 13.0 Hz, 1H), 6.84 (d, J = 8.7 Hz, 1H), 6.88 (dd, J = 2.8 Hz, 8.7 Hz, 1H), 6.92−6.95 (m, 1H), 6.97 (d, J = 2.6 Hz, 1H), 7.08−7.10 (m, 2H), 7.31−7.35 (m, 1H); ^{13}C NMR (DMSO-d_6, 400 MHz): δ44.1, 55.1, 78.5, 79.2, 108.5, 112.1, 113.7, 118.2, 118.6, 120.8, 123.5, 129.6, 141.0, 143.1, 152.7, 159.3, 191.9.

*General Synthesis of Galloyl Conjugates of Flavanones (**5a−n**).* The respective amines (0.01 mol) thus obtained were dissolved in dichloromethane at 0 °C followed by slow addition of triethylamine (0.15 mol). This reaction mixture was then allowed to stir for 15 min, and a solution of 3,4,5-trimethoxybenzoyl chloride (0.01 mol) in dichloromethane was added slowly. The resulting reaction mixture was then stirred at room temperature for 2 h. On completion, the usual workup was done followed by purification of the crude residue obtained by column chromatography using ethylacetate/hexane as an eluent.

*N-(2-(2,4-Dichlorophenyl)-4-oxochroman-6-yl)-3,4,5-trimethoxybenzamide (**5a**).* Yellow solid; yield: 74%; mp: 203−205 °C; ^{1}H NMR ($CDCl_3$, 400 MHz): δ 2.85 (dd, J = 13.5 Hz, 17.0 Hz, 1H), 3.02 (dd, J = 2.8 Hz, 17.0 Hz, 1H), 3.91 (s, 3H), 3.94 (s, 6H), 5.82 (dd, J = 2.8 Hz, 13.5 Hz, 1H), 7.11 (s, 2H), 7.13 (s, 1H), 7.39 (dd, J = 2.1 Hz, 8.4 Hz, 1H), 7.45 (d, J = 2.0 Hz, 1H), 7.70 (d, J = 8.4 Hz, 1H), 7.87 (d, J = 2.7 Hz, 1H), 7.91 (s, 1H), 8.16 (dd, J = 2.8 Hz, 9.0 Hz, 1H); ^{13}C NMR ($CDCl_3$, 400 MHz): δ43.4, 56.5, 61.1, 76.4, 104.8, 118.2, 119.0, 120.8, 128.0, 128.3, 129.7, 129.9, 130.0, 132.4,132.8, 135.1, 135.4, 141.6, 153.5, 158.3, 165.8, 191.2; ESI-MS (m/z): 502 $[M + H]^+$; HRMS m/z calcd for $C_{25}H_{22}Cl_2NO_6$ $[M + H]^+$ 502.0824, found 502.0820.

*N-(2-(3-Fluorophenyl)-4-oxochroman-6-yl)-3,4,5-trimethoxybenzamide (**5b**).* Yellow solid; yield: 72%; mp: 217−219 °C; ^{1}H NMR ($CDCl_3$, 400 MHz): δ2.90 (dd, J = 3.0 Hz, 16.9 Hz, 1H), 3.24−3.28 (m, 1H), 3.74 (s, 3H), 3.88 (s, 6H), 5.72 (dd, J = 2.8 Hz, 12.8 Hz, 1H), 7.17 (d, J = 9.0 Hz, 1H), 7.21−7.26 (m, 1H), 7.31 (s, 2H), 7.40−7.44 (m, 2H), 7.47−7.52 (m, 1H), 7.99 (dd, J = 2.7 Hz, 9.0 Hz, 1H), 8.18 (d, J = 2.7 Hz, 1H), 10.20 (s, 1H); ^{13}C NMR ($CDCl_3$, 400 MHz): δ43.4, 56.1, 60.1, 78.1, 105.3, 113.3, 113.5, 115.2, 115.3, 117.6, 118.2, 120.3, 122.6, 129.3, 129.6, 130.6, 130.7, 133.1, 140.4, 141.7, 152.6, 157.1, 161.2, 163.1, 164.6, 191.2; ESI-MS (m/z): 452 $[M + H]^+$; HRMS m/z calcd for $C_{25}H_{23}FNO_6$ $[M + H]^+$ 452.1509, found 452.1503.

*3,4,5-Trimethoxy-N-(4-oxo-2-(m-tolyl)chroman-6-yl)benzamide (**5c**).* Yellow solid; yield: 80%; mp: 191−193 °C; ^{1}H NMR ($CDCl_3$, 400 MHz): δ2.40 (s, 3H), 2.86 (dd, J = 3.0 Hz, 17.0 Hz, 1H), 3.08 (dd, J = 13.4 Hz, 17.0 Hz, 1H), 3.89 (s, 3H), 3.92 (s, 6H), 5.44 (dd, J = 2.8 Hz, 13.3 Hz, 1H), 7.09 (d, J = 9.0 Hz, 1H), 7.11 (s, 2H), 7.21 (d, J = 7.5 Hz, 1H), 7.27−7.34 (m, 3H), 7.86 (d, J = 2.7 Hz, 1H), 8.07 (s, 1H), 8.13 (dd, J = 2.8 Hz, 9.3 Hz, 1H); ^{13}C NMR ($CDCl_3$, 400 MHz): δ21.6, 44.6, 56.5, 60.5, 61.0, 79.9, 104.9, 118.2, 119.0, 120.8, 123.4, 127.0, 128.9, 129.7, 129.9, 130.0, 132.4, 138.6, 138.8, 141.5, 153.4, 158.6, 165.9, 192.2; ESI-MS (m/z): 487 $[M + K]^+$; HRMS m/z calcd for $C_{26}H_{26}NO_6$ $[M + H]^+$ 448.1760, found 448.1753.

*N-(2-(3-Hydroxyphenyl)-4-oxochroman-6-yl)-3,4,5-trimethoxybenzamide (**5d**).* Yellow solid; yield: 79%; mp: 111−113 °C; ^{1}H NMR (DMSO-d_6, 400 MHz): δ2.83 (dd, J = 2.9 Hz, 16.8 Hz, 1H), 3.19 (dd, J = 12.6 Hz, 16.8 Hz, 1H), 3.74 (s, 3H), 3.88 (s, 6H), 5.59 (dd, J = 2.9 Hz, 12.6 Hz, 1H), 6.76−6.78 (m, 1H), 6.93−6.95 (m, 2H), 7.13 (d, J = 9.0 Hz, 1H), 7.22 (t, J = 8.2 Hz, 1H), 7.31 (s, 2H), 7.99 (dd, J = 2.8 Hz, 9.0 Hz, 1H), 8.17 (d, J = 2.7 Hz, 1H), 9.67 (brs, 1H), 10.20 (s, 1H); ^{13}C NMR (DMSO-d_6, 400 MHz): δ43.6, 56.1, 60.1, 78.8, 105.3, 113.4, 115.4, 117.0, 117.6, 118.1, 120.4, 129.3, 129.6, 129.7, 133.0, 140.4, 152.7, 157.3, 157.6, 164.7, 191.6; ESI-MS (m/z): 450 $[M + H]^+$; HRMS m/z calcd for $C_{25}H_{24}NO_7$ $[M + H]^+$ 450.1553, found 450.1548.

*3,4,5-Trimethoxy-N-(2-(3-methoxyphenyl)-4-oxochroman-6-yl)-benzamide (**5e**).* Yellow solid; yield: 84%; mp: 171−173 °C; ^{1}H NMR ($CDCl_3$, 400 MHz): δ2.89 (dd, J = 3.0 Hz, 17.0 Hz, 1H), 3.07 (dd, J = 13.2 Hz, 17.0 Hz, 1H), 3.85 (s, 3H), 3.90 (s, 3H), 3.93 (s, 6H), 5.46 (dd, J = 2.8 Hz, 13.2 Hz, 1H), 6.91−6.94 (m, 1H), 7.04−7.05 (m, 2H), 7.10 (fused d, 1H), 7.11 (s, 2H), 7.35 (t, J = 8.1 Hz, 1H), 7.85 (d, J = 2.7 Hz, 1H), 8.00 (s, 1H), 8.15 (dd, J = 2.8 Hz, 9.0 Hz, 1H); ^{13}C NMR ($CDCl_3$, 400 MHz): δ44.7, 55.5, 56.5, 61.1, 79.7, 104.8, 112.0, 114.3, 118.2, 118.4, 119.0, 120.8,129.9, 130.0, 130.1, 132.4, 140.2, 141.5, 153.4, 158.5, 160.1, 165.7, 192.0; ESI-MS (m/z): 464 $[M + H]^+$; HRMS m/z calcd for $C_{26}H_{26}NO_7$ $[M + H]^+$464.1709, found 464.1705.

*N-(2-(4-Chlorophenyl)-4-oxochroman-6-yl)-3,4,5-trimethoxybenzamide (**5f**).* Yellow solid; yield: 78%; mp: 218−220 °C; ^{1}H NMR (DMSO-d_6, 400 MHz): δ2.87 (dd, J = 2.9 Hz, 16.8 Hz, 1H), 3.26 (dd, J = 12.9 Hz, 16.8 Hz, 1H),3.74 (s, 3H), 3.88 (s, 6H), 5.71 (dd, J = 2.8 Hz, 13.0 Hz, 1H), 7.15 (d, J = 8.9 Hz, 1H), 7.31 (s, 2H), 7.51 (d, J = 8.5 Hz, 2H), 7.60 (d, J = 8.5 Hz, 2H), 7.99 (dd, J = 2.6 Hz, 8.9 Hz, 1H), 8.18 (d, J = 2.6 Hz, 1H), 10.19 (s, 1H); ^{13}C NMR ($CDCl_3$, 400 MHz): δ43.4, 56.1, 60.1, 78.1, 105.3, 117.5, 118.1, 120.3, 128.5, 128.5, 129.2, 129.6, 133.1, 138.0, 140.4, 152.6, 157.2, 164.6, 191.3; ESI-MS (m/z): 468 $[M + H]^+$; HRMS m/z calcd for $C_{25}H_{23}ClNO_6$ $[M + H]^+$468.1214, found 468.1208.

*Ethyl 4-(4-Oxo-6-(3,4,5-trimethoxybenzamido)chroman-2-yl)-benzoate (**5g**).* Yellow solid; yield: 76%; mp 177−179 °C; ^{1}H NMR ($CDCl_3$, 400 MHz): δ1.41 (t, J = 7.2 Hz, 3H), 2.92 (dd, J = 3.2 Hz, 17.0 Hz, 1H), 3.05 (dd, J = 12.9 Hz, 16.9 Hz, 1H), 3.90 (s, 3H), 3.93 (s, 6H), 4.40 (q, J = 7.2 Hz, 2H), 5.56 (dd, J = 3.3 Hz, 13.0 Hz, 1H), 7.11 (s, 2H), 7.12 (fused d, 1H), 7.56 (d, J = 2.8 Hz, 2H), 7.86 (d, J = 2.7 Hz, 1H), 8.10−8.16 (m, 3H); ^{13}C NMR ($CDCl_3$, 400 MHz): δ14.4, 44.6, 56.5, 61.0, 61.3, 79.2, 104.9, 118.2, 119.0, 120.8, 126.0, 130.0, 130.2, 131.0, 132.7, 141.5, 143.4, 153.4, 158.2, 165.8, 166.2, 191.4; ESI-MS (m/z): 506 $[M + H]^+$; HRMS m/z calcd for $C_{28}H_{28}NO_8$$[M + H]^+$ 506.1815, found 506.1802.

*N-(2-(4-Ethylphenyl)-4-oxochroman-6-yl)-3,4,5-trimethoxybenzamide (**5h**).* Yellow solid; yield: 81%; mp: 178−180 °C; ^{1}H NMR ($CDCl_3$, 400 MHz): δ1.26 (t, J = 7.4 Hz, 3H), 2.68 (q, J = 7.5 Hz, 2H), 2.84 (dd, J = 2.0 Hz, 16.8 Hz, 1H), 3.07 (dd, J= 13.1 Hz, 16.8 Hz, 1H), 3.87 (s, 3H), 3.90 (s, 6H), 5.43 (d, J = 11.7 Hz, 1H), 7.05 (d, J = 9 Hz, 1H), 7.13 (s, 2H), 7.25−7.27 (m, 2H), 7.38 (d, J = 7.8 Hz, 2H), 7.87 (s, 1H), 8.13 (d, J = 7 Hz, 1H), 8.28 (s, 1H); ^{13}C NMR ($CDCl_3$, 400 MHz): δ15.6, 28.7, 44.5, 56.5, 61.0, 79.8, 104.9, 118.2, 119.0, 120.8, 126.4, 128.5, 130.0, 130.0, 132.4, 135.8, 141.4, 145.3, 153.4, 158.7,

https://doi.org/10.1021/acs.jmedchem.1c00112
J. Med. Chem. XXXX, XXX, XXX−XXX

165.8, 192.3; ESI-MS (m/z): 462 $[M + H]^+$; HRMS m/z calcd for $[M + H]^+$ $C_{27}H_{28}NO_6$ 462.1917, found 462.1909.

*N-(2-(4-Fluorophenyl)-4-oxochroman-6-yl)-3,4,5-trimethoxybenzamide (**5i**).* Yellow solid; yield: 74%; mp: 215−217 °C; ^{1}H NMR (DMSO-d_6, 400 MHz): δ2.83−2.87 (m, 1H), 3.26−3.33 (m, 1H), 3.74 (s, 3H), 3.88 (s, 6H), 5.68−5.70 (m, 1H), 7.13−7.15 (m, 3H), 7.31 (s, 2H), 7.63 (s, 2H), 7.98−8.00 (m, 1H), 8.19 (s, 1H), 10.20 (s, 1H); ^{13}C NMR (DMSO-d_6, 400 MHz): δ43.6, 56.2, 60.2, 78.3, 105.3, 115.3, 115.5, 117.7, 118.2, 120.3, 129.0, 129.0, 129.3, 129.7, 133.1, 135.3, 140.4, 152.7, 157.4, 160.9, 163.3, 164.8, 191.6; ESI-MS (m/z): 452 $[M + H]^+$; HRMS m/z calcd for $C_{25}H_{23}FNO_6$ $[M + H]^+$ 452.1509, found 452.1506.

*N-(2-(4-Isopropylphenyl)-4-oxochroman-6-yl)-3,4,5-trimethoxybenzamide (**5j**).* Yellow solid; yield: 79%; mp: 186−189 °C; ^{1}H NMR ($CDCl_3$, 400 MHz): δ1.27 (d, J = 6.9 Hz, 6H), 2.89 (dd, J = 3.0 Hz, 17.0 Hz, 1H), 2.96 (q, J = 6.9 Hz, 1H), 3.12 (dd, J = 13.3 Hz, 16.9 Hz, 1H), 3.90 (s, 3H), 3.93 (s, 6H), 5.46 (dd, J = 2.7 Hz, 13.3 Hz, 1H), 7.09 (fused d, 1H), 7.10 (s, 2H), 7.30 (d, J = 8.2 Hz, 2H), 7.41 (d, J = 8.1 Hz, 2H), 7.85 (d, J = 2.7 Hz, 1H), 7.90 (s, 1H), 8.12 (dd, J = 2.7 Hz, 9.0 Hz, 1H); ^{13}C NMR ($CDCl_3$, 400 MHz): δ24.1, 34.1, 44.5, 56.6, 61.1, 79.8, 104.9, 118.2, 119.0, 120.9, 126.4, 127.1, 129.9, 130.1, 132.3, 136.0, 141.6, 150.0, 153.5, 158.7, 165.8, 192.3; ESI-MS (m/z): 476 $[M + H]^+$; HRMS m/z calcd for $C_{28}H_{30}NO_6$ $[M + H]^+$ 476.2073, found 476.2063.

*3,4,5-Trimethoxy-N-(4-oxo-2-(p-tolyl)chroman-6-yl)benzamide (**5k**).* Yellow solid; yield: 81%; mp: 195−198 °C; ^{1}H NMR ($CDCl_3$, 400 MHz): δ2.39 (s, 3H), 2.87 (dd, J = 2.9 Hz, 17.0 Hz, 1H), 3.09 (dd, J = 13.1 Hz, 16.9 Hz, 1H), 3.90 (s, 3H), 3.93 (s, 6H), 5.45 (dd, J = 2.7 Hz, 13.2 Hz, 1H), 7.09 (d, J = 9.1 Hz, 1H), 7.10 (s, 2H), 7.25 (d, J = 8.2 Hz, 1H), 7.37 (d, J = 8.0 Hz, 2H), 7.85 (d, J = 2.5 Hz, 1H), 7.93 (s, 1H), 8.13 (dd, J = 2.5 Hz, 8.9 Hz, 1H); ^{13}C NMR ($CDCl_3$, 400 MHz): δ21.3, 44.5, 56.5, 61.1, 79.8, 104.9, 118.2, 119.0, 120.8, 126.3, 129.6, 129.9, 130.0, 132.4, 135.6, 139.0, 141.5, 153.4, 158.7, 165.8, 192.3; ESI-MS (m/z): 448 $[M + H]^+$; HRMS m/z calcd for $C_{26}H_{26}NO_6$ $[M + H]^+$ 448.1760, found 448.1749.

*3,4,5-Trimethoxy-N-(4-oxo-2-phenylchroman-6-yl)benzamide (**5l**).* Yellow solid; yield: 80%; mp: 242−246 °C; ^{1}H NMR (DMSO-d_6, 400 MHz): δ2.87 (dd, J = 2.8 Hz, 16.9 Hz, 1H), 3.25−3.29 (m, 1H), 3.74 (s, 3H), 3.88 (s, 6H), 5.69 (dd, J = 2.9 Hz, 13.0 Hz, 1H), 7.15 (d, J = 8.9 Hz, 1H), 7.31 (s, 2H), 7.38−7.47 (m, 3H), 7.57 (d, J = 7.0 Hz, 2H), 7.99 (dd, J = 2.6 Hz, 8.9 Hz, 1H), 8.19 (d, J = 2.7 Hz, 1H), 10.20 (s, 1H); ^{13}C NMR (DMSO-d_6, 400 MHz): δ43.6, 56.1, 60.2, 78.9, 105.3, 117.6, 118.2, 120.3, 126.6, 128.6, 129.3, 129.6, 133.0, 139.0, 140.4, 152.7, 157.4, 164.7, 191.6; ESI-MS (m/z): 434 $[M + H]^+$; HRMS m/z calcd for $C_{25}H_{24}NO_6$ $[M + H]^+$ 434.1604, found 434.1590.

*3,4,5-Trimethoxy-N-(4-oxo-2-(thiophen-3-yl)chroman-6-yl)-benzamide (**5m**).* Yellow solid; yield: 78%; mp: 230−235 °C; ^{1}H NMR (DMSO-d_6, 400 MHz): δ2.97 (dd, J = 3.2 Hz, 16.9 Hz, 1H), 3.25−3.30 (m, 1H), 3.74 (s, 3H), 3.88 (s, 6H), 5.74 (dd, J = 3.1 Hz, 13.9 Hz, 1H), 7.12 (d, J = 9.0 Hz, 1H), 7.29−7.31 (m, 1H), 7.32 (s, 2H), 7.59−7.61 (m, 1H), 7.64−7.65 (m, 1H), 7.99 (dd, J = 2.7 Hz, 9.0 Hz, 1H), 8.18 (d, J = 2.6 Hz, 1H), 10.24 (s, 1H); ^{13}C NMR (DMSO, 400 MHz): δ42.9, 56.1, 60.1, 75.0, 105.3, 117.5, 118.1, 120.3, 123.6, 126.4, 127.0, 129.2, 129.6, 133.0, 140.1, 140.4, 152.6, 157.1, 164.6, 191.4; ESI-MS (m/z): 440 $[M + H]^+$; HRMS m/z calcd for $C_{23}H_{22}NO_6S$ $[M + H]^+$ 440.1168, found 440.1165.

*N-(2-(4-(tert-Butyl)phenyl)-4-oxochroman-6-yl)-3,4,5-trimethoxybenzamide (**5n**).* Yellow solid; yield: 78%; mp: 169−172 °C; ^{1}H NMR ($CDCl_3$, 400 MHz): δ1.34 (s, 9H), 2.82−2.90 (m, 2H), 2.98−3.13 (m, 2H), 3.87 (s, 3H), 3.88 (s, 1H), 3.90 (s, 6H), 3.91 (s, 6H), 5.44 (dd, J = 2.8 Hz, 13.3 Hz, 1H), 5.86 (dd, J = 2.9 Hz, 13.4 Hz, 1H), 7.06 (d, J = 8.9 Hz, 1H), 7.09 (d, J = 8.9 Hz, 1H), 7.13 (s, 2H), 7.14 (s, 2H), 7.30−7.38 (m, 2H), 7.40−7.42 (m, 4H), 7.45−7.47 (m, 2H), 7.73−7.76 (m, 1H), 7.87 (d, J = 2.7 Hz, 1H), 7.89 (d, J = 2.7 Hz, 1H), 8.13 (dd, J = 2.7 Hz, 9.0 Hz, 1H), 8.17 (dd, J = 2.7 Hz, 9.0 Hz, 1H), 8.25 (s, 1H), 8.28 (s, 1H); ^{13}C NMR ($CDCl_3$, 400 MHz): δ29.8, 31.4, 34.8, 43.5, 44.4, 56.5, 61.0, 79.7, 104.9, 118.2, 118.3, 118.9, 120.8, 120.8, 125.9, 126.2, 127.4, 129.8, 129.9, 129.9, 130.0, 130.0, 131.8, 132.4, 132.7, 135.5, 136.7, 141.5, 141.5, 152.2, 153.4, 158.5, 158.7, 165.8, 191.7, 192.3; ESI-MS (m/z): 490 $[M + H]^+$; HRMS m/z calcd for $C_{29}H_{32}NO_6$ $[M + H]^+$ 490.2230, found 490.2221.

*General Synthesis of Galloyl Conjugates of Flavan-4-ols (**6o−t**).* The respective galloyl conjugate of flavanone **5** (1.0 mmol) was taken in methanol (10 mL) followed by treatment with an excess of $NaBH_4$ (1.5 mmol) at 0 °C. The resulting reaction mixture was allowed to stir at room temperature for 30 min. On completion of the reaction as monitored by TLC, the reaction mixture was then concentrated in a high vacuum. The remaining residue was dispersed in water and extracted with dichloromethane. Thus-obtained organic layers were combined, dried over anhydrous sodium sulfate, and finally concentrated in a vacuum to yield the desired compound (**6o−t**) in the pure form.

*N-(2-(3-Fluorophenyl)-4-hydroxychroman-6-yl)-3,4,5-trimethoxybenzamide (**6o**).* White solid; yield: 88%; mp: 159−161 °C; ^{1}H NMR (DMSO-d_6, 400 MHz): δ1.93 (q, J = 12.0 Hz, 1H), 2.32−2.38 (m, 1H), 3.73 (s, 3H), 3.87 (s, 6H), 4.95−4.99 (m, 1H), 5.29 (d, J = 10.8 Hz, 1H), 5.63 (s, 1H), 6.81 (d, J = 8.7 Hz, 1H), 7.16−7.21 (m, 1H), 7.29−7.31 (m, 1H), 7.31 (s, 2H), 7.32−7.34 (m, 2H), 7.44−7.50 (m, 1H), 7.57 (dd, J = 2.5 Hz, 8.8 Hz, 1H), 7.81 (d, J = 2.1 Hz, 1H), 10.04 (s, 1H); ^{13}C NMR (DMSO-d_6, 400 MHz): δ56.1, 60.1, 63.9, 75.7, 79.2, 105.2, 112.8, 112.9, 114.7, 115.6, 120.1, 121.4, 122.1, 127.3, 130.0, 130.4, 130.5, 132.0, 140.2, 144.0, 150.2, 152.6, 164.3; ESI-MS (m/z): 440 $[M + H]^+$; HRMS m/z calcd for $C_{25}H_{25}FNO_6$ $[M + H]^+$ 454.1666, found 454.1654.

*N-(4-Hydroxy-2-(m-tolyl)chroman-6-yl)-3,4,5-trimethoxybenzamide (**6p**).* White solid; yield: 86%; mp: 156−158 °C; ^{1}H NMR (DMSO-d_6, 400 MHz): δ1.96 (q, J = 12.1 Hz, 1H), 2.28−2.32 (m, 1H), 2.35 (s, 1H), 3.73 (s, 3H), 3.87 (s, 6H), 4.96−5.00 (m, 1H), 5.20 (d, J = 11.0 Hz, 1H), 5.55 (d, J = 7.0 Hz, 1H), 6.51 (s, 1H), 6.78 (d, J = 8.7 Hz, 1H), 7.16 (d, J = 7.2 Hz, 1H), 7.24−7.28 (m, 2H), 7.30 (s, 2H), 7.55 (dd, J = 2.5 Hz, 8.7 Hz, 1H), 7.79 (d, J = 2.1 Hz, 1H), 10.00 (s, 1H); ^{13}C NMR (DMSO-d_6, 400 MHz): δ21.1, 56.1, 60.1, 64.1, 76.5, 105.2, 115.6, 120.1, 121.4, 123.3, 126.7, 127.3, 128.3, 128.5, 130.1, 131.8, 137.6, 140.1, 141.0, 150.6, 152.6, 164.3; ESI-MS (m/z): 450 $[M + H]^+$; HRMS m/z calcd for $C_{26}H_{28}NO_6$ $[M + H]^+$ 450.1917, found 450.1909.

*N-(4-Hydroxy-2-(3-methoxyphenyl)chroman-6-yl)-3,4,5-trimethoxybenzamide (**6q**).* White solid; yield: 87%; mp: 167−169 °C; ^{1}H NMR (DMSO-d_6, 400 MHz): δ1.96 (q, J = 12.0 Hz, 1H), 2.30−2.35 (m, 1H), 3.73 (s, 3H), 3.78 (s, 1H), 3.87 (s, 6H), 4.94−5.00 (m, 1H), 5.22 (d, J = 11.3 Hz, 1H), 5.56 (d, J = 7 Hz, 1H), 6.79 (d, J = 8.7 Hz, 1H), 7.92 (dd, J = 2.1, 8.2 Hz, 1H), 7.03−7.06 (m, 2H), 7.31 (s, 2H), 7.31−7.35 (m, 1H), 7.55 (dd, J = 2.6 Hz, 8.7 Hz, 1H), 7.80 (d, J = 2.3 Hz, 1H), 10.00 (s, 1H); ^{13}C NMR (DMSO-d_6, 400 MHz): δ55.1, 56.1, 60.1, 64.0, 76.4, 105.2, 111.7, 113.3, 115.6, 118.2, 120.1, 121.4, 127.3, 129.5, 130.0, 131.9, 140.2, 142.6, 150.5, 152.6, 159.3, 164.3; ESI-MS (m/z): 466 $[M + H]^+$; HRMS m/z calcd for $C_{26}H_{28}NO_7$ $[M + H]^+$ 466.1866, found 466.1860.

*N-(2-(4-Chlorophenyl)-4-hydroxychroman-6-yl)-3,4,5-trimethoxybenzamide (**6r**).* White solid; yield: 88%; mp: 117−119 °C; ^{1}H NMR (DMSO-d_6, 400 MHz): δ1.93 (q, J = 12.0 Hz, 1H), 2.31−2.35 (m, 1H), 3.73 (s, 3H), 3.87 (s, 6H), 5.00 (m, 1H), 5.26−5.29 (m, 1H), 5.58−5.60 (m, 1H), 6.51 (s, 1H), 6.80 (d, J = 8.7 Hz, 1H), 7.30 (s, 2H), 7.47−7.57 (m, 5H), 7.80 (d, J = 2.1 Hz, 1H), 10.00 (s, 1H); ^{13}C NMR (DMSO-d_6, 400 MHz): δ56.1, 60.1, 63.9, 75.7, 105.2, 115.6, 120.1, 121.4, 127.3, 128.0, 128.4, 130.0, 132.0, 140.0, 140.2, 150.3, 152.6, 164.3; ESI-MS (m/z): 470 $[M + H]^+$; HRMS m/z calcd for $C_{25}H_{25}ClNO_6$ $[M + H]^+$ 470.1370, found 470.1360.

*N-(4-Hydroxy-2-phenylchroman-6-yl)-3,4,5-trimethoxybenzamide (**6s**).* White solid; yield: 85%; mp: 152−154 °C; ^{1}H NMR (DMSO-d_6, 400 MHz): δ1.92−2.01 (m, 1H), 2.30−2.35 (m, 1H), 3.73 (s, 3H), 3.87 (s, 6H), 4.95−5.04 (m, 1H), 5.25 (d, J = 10.0 Hz, 7.0 Hz, 1H), 5.57 (d, J = 6.8 Hz, 1H), 6.78 (d, J = 8.8 Hz, 1H), 7.31 (s, 2H), 7.33−7.38 (m, 1H), 7.40−7.44 (m, 2H), 7.7−7.50 (m, 2H), 7.56 (dd, J = 2.5 Hz, 8.7 Hz, 1H), 7.80 (d, J = 2.1 Hz, 1H), 10.01 (s, 1H); ^{13}C NMR (DMSO-d_6, 400 MHz): δ56.1, 60.1, 64.0, 76.5, 79.2, 105.2, 115.5, 120.1, 121.4, 126.2, 127.3, 127.9, 128.4, 130.0, 131.9, 140.1, 141.0, 150.5, 152.6, 164.3; ESI-MS (m/z): 475 $[M + K + H]^+$; HRMS m/z calcd for $C_{25}H_{26}NO_6$ $[M + H]^+$ 436.1760, found 436.1747.

*N-(2-(4-(tert-Butyl)phenyl)-4-oxochroman-6-yl)-3,4,5-trimethoxybenzamide (**6t**).* White solid; yield: 85%; mp: 147−149 °C; ^{1}H NMR (DMSO-d_6, 400 MHz): δ1.30 (s, 9H), 1.86−2.03 (m, 2H), 2.28−2.33

https://doi.org/10.1021/acs.jmedchem.1c00112
J. Med. Chem. XXXX, XXX, XXX−XXX

(m, 1H), 2.38−2.43 (m, 1H), 3.73 (s, 6H), 3.87 (s, 12H), 4.96−5.04 (m, 2H), 5.20 (d, J = 10.7 Hz, 1H), 5.52−5.56 (m, 2H), 5.64 (d,J = 6.6 Hz, 1H), 6.51 (s, 1H), 6.76 (d, J = 8.7 Hz, 1H), 6.83 (d, J = 8.8 Hz, 1H), 7.29−7.31 (m, 4H), 7.38−7.47 (m, 6H), 7.51 (dd, J = 1.4 Hz, 7.7 Hz, 1H), 7.56 (dd, J = 2.5 Hz, 8.7 Hz, 1H), 7.59 (dd, J = 2.5 Hz, 8.8 Hz, 1H), 7.67 (dd, J = 1.7 Hz, 7.6 Hz, 1H), 7.81 (dd, J = 2.2 Hz, 7.1 Hz, 2H), 9.10 (s, 1H), 10.24 (s, 1H); ^{13}C NMR (DMSO-d_6, 400 MHz): δ 31.1, 34.3, 37.8, 56.1, 60.1, 63.9, 64.1, 73.5, 76.4, 105.2, 115.5, 115.6, 120.1, 120.2, 121.4, 121.5, 125.1, 126.0, 127.2, 127.3, 127.5, 127.7, 129.5, 129.6, 130.0, 130.0, 131.0, 131.8, 132.1, 138.0, 138.1, 140.2, 140.2, 150.2, 150.4, 150.6, 152.6, 164.3, 164.3; ESI-MS (m/z): 492 $[M + H]^+$; HRMS m/z calcd for $C_{29}H_{34}NO_6$ $[M + H]^+$ 492.2386, found 492.2373.

Chiral Separation of 5e. Racemic **5e** was subjected to chiral separation over normal-phase Shimadzu HPLC with a PDA detector using an analytical Chiralpak IA column (4.6 mm × 250 mm, 5 μm mesh size) and eluted with isocratic solvent system isopropyl alcohol and n-hexane in the ratio 2:8 at the flow rate of 1 mL/min; two peaks were resolved with retention times at 15.17 and 32.54 min. With the optimized method in hand, pure R and S isomers were obtained with preparative HPLC using a Chiralpak IA column (20 mm × 250 mm, 5 μm mesh size).

CD Spectroscopy. CD spectra for **5e** isomers were recorded at 25 °C using a J-1500, JASCO CD spectrophotometer. Samples were prepared in methanol with 2 μM concentration, and the final values were obtained from the average of three consecutive scans with solvent subtraction. CD values were obtained as degrees of ellipticity "θ" in mdeg against wavelength in nm.

Biological Assays. *Rat Calvaria Osteoblast Culture (RCO).* The primary cell population of osteoblast was obtained by sequential enzymatic digestion of the calvarial bone matrix. Rat pups (1 or 2 days old) were used for the isolation of cells. Institutional Animal Ethics Committee approval was obtained (IAEC/2020/65). Calvariae of pups were isolated, sutures were segregated, and adherent tissues were discarded by scrapping, and cleaned calvariae were crumbled. An enzyme cocktail of Dispase II (1 mg/mL) and Collagenase type-P (1 mg/mL) was prepared. Crumbled calvaria was incubated at 37 °C in the enzyme cocktail for five consecutive digestions (15 min/digestion) to release the cells. The supernatant from the first digestion was discarded, and cells were collected from the 2nd to 5th digestions, in a complete α-MEM medium containing 10% fetal bovine serum (FBS) and 1% antibiotic-antimycotic solution.

Alkaline Phosphatase Assay. Rat calvarial osteoblasts were trypsinized after attainment of 70−80% confluency, and 2 × 10^3 cells/well were seeded in 96-well plates to assess the ALP activity. Once the desired confluency was obtained, cells were treated with different concentrations of 20 test compounds for 48 h in α-MEM supplemented with 10% FBS, 10 mM β-glycerophosphate, 50 μg/mL ascorbic acid, and 1% penicillin/streptomycin (osteoblast differentiation medium). At the end of the incubation period, media were evacuated and PBS was added to wash out. Plates were kept at −80 °C overnight and then incubated at 37 °C to induce rupturing of the cells. The total ALP activity was measured using p-nitrophenyl phosphate (PNPP) as the substrate, and absorbance was taken at 405 nm.

Cell Viability Assay. The toxicity of compounds was tested on calvarial osteoblast cells. Cells were seeded in a 96-well plate (2 × 10^3 cells/well) for 24 h at 37 °C and 5% CO_2. Once the confluency reaches 70−80%, cells were treated with various concentrations of **6p, 5e, 5n**, and **5l** compounds ranging from 1 pM to 1 μM in 10% proliferating (α-MEM with 10% FBS, 1% antibiotic and antimycotic). After 48 h, 10 μL of MTT solution (5 mg/mL) was added to each well for 4 h at 37 °C. Formazan crystals were dissolved by adding 100 μL of dimethyl sulfoxide (DMSO) in each well after the removal of media, and the OD was taken at 570 nm.

Mineralized Nodule Formation Assay. Upon differentiation induction calvarial osteoblast display efficient mineralizing ability. To analyze this activity, cells were seeded onto 12-well plates (10 000 cells/well). In a 10% osteoblast differentiation medium, osteoblasts were treated with or without test compounds for 14 days at different concentrations and in triplicates; after every 48 h, fresh media along with the compound were supplied to the cells. At the end of the experiment, cells were washed with phosphate-buffered saline (PBS) and fixed with 4% paraformaldehyde in PBS for 15 min. The fixed cells were stained with Alizarin red-S (40 mM, pH 4.5) for 30 min followed by washing with tap water. Stained cells that appear as mineralized nodules were photographed by a camera (Canon SX410). For quantification of mineralized nodules, Cetylpyridinium chloride method was taken into account. Briefly, 500 μL of 10% (w/v) CPC was added in a plate and incubated for 1 h. After the end of the incubation period, the dye solution was transferred in a 96-well plate and absorbance was taken at 595 nm.

Quantitative Real-Time Polymerase Chain Reaction (qPCR) for RCO In Vitro Study. Cells were treated with different concentrations of test compounds **6p**, **5e**, **5n**, and **5l** for 48 h. At the end of the treatment, cells were collected in QIAazol (Qiagen) and the total RNA was isolated according to the manufacturer's protocol. The qPCR reaction was performed for quantitative comparative measurement of the expression of osteoblast-specific genes ALP, ColI, BMP-2, and RUNX2 following an optimized protocol using a high-capacity cDNA reverse transcription kit (Thermo Fisher) using 2.0 μg of total RNA. The housekeeping gene GAPDH was used as an internal control. Primers were designed using the Universal Probe Library (Roche Applied Sciences) for the selected genes (Table 1). SYBR Green chemistry was used to perform quantitative determination of the relative expression of transcripts for all genes. All genes were analyzed using the Quant Studio 3 (Applied Biosystem Foster City, California) real-time PCR machine.[44]

Western Blot Analysis. Cells were seeded in a T-25 flask for 24 h to reach approximately 70−80% confluency. Treatment of our lead compound (**5e**) was performed at three different concentrations (1, 10, and 100 pM) for 48 h in a 10% osteoblast differentiating medium. Cells were washed with cold PBS, and lysates were prepared using a RIPA buffer containing a protease and phosphatase inhibitor mixture. A total of 30 μg of cell lysates was separated on sodium dodecyl sulfate polyacrylamide gel electrophoresis (SDS-PAGE) under reducing conditions (Bio-Rad, Hercules, CA) and then transferred to poly-(vinylidene difluoride) (PVDF) membranes (Millipore, Watford, U.K.). Membranes were blocked by 5% BSA and then kept at 4 °C overnight with the primary antibody BMP-2 (ab-14933, dilution 1:1000), RUNX2 (12 556s, dilution 1:1000), p-Smad 1 (ab-63439, dilution 1:1000), Smad 1 (SC-7965, dilution 1:1000), and β-actin (A3854, dilution 1:50 000). After overnight incubation, membranes were washed with a wash buffer (PBST) thrice with gentle shaking and probed with an HRP conjugated secondary antibody at room temperature for 2 h, and then, western blot signals were visualized by a chemiluminescence system (GE Healthcare Life Sciences, Bangalore, India) according to the manufacturer's instructions.[45]

In Vivo Calvarial Injection and qPCR. To establish the potency of compound **5e** *in vivo*, 7 day old rat pups with their mother were taken. Pups were divided into four groups (n = 5/group), namely, Vehicle, 1 mg/kg, 5 mg/kg, and 10 mg/(kg day) body weight. Lead compound **5e** was injected subcutaneously in the pup's calvaria for 6 days. After the end of the experimental time point, pups were euthanized and calvariae were separated by making a straight cut across the sagittal suture and collected in chilled PBS. Calvariae were homogenized with QIAazol (Qiagen), and RNA was isolated according to the manufacturer's protocol. Further, cDNA was synthesized by a high-capacity cDNA reverse transcription kit with random primers. Gene expressions of BMP-2, RUNX2, OCN, and Col1 were assessed using Power up SYBR Green in Applied Biosystem Quantstudio3 RT-PCR. GAPDH was taken as an endogenous control.[35]

Calvarial Histomorphometry. Dynamic bone indices were evaluated from fluorescein (5 mg/kg)[35] given at an interval of 5 day double-labeled calvaria sectioned at 50 μm using an Isomet bone cutter and photographed under a fluorescent microscope. Briefly, the calvariae were embedded in an acrylic material for the determination and calculation of the bone formation rate/bone surface (BFR/BS) and the mineral appositional rate (MAR) using Leica IM50 Image Acquisition software following a previously described protocol, and analysis was done using Image pro software.

https://doi.org/10.1021/acs.jmedchem.1c00112
J. Med. Chem. XXXX, XXX, XXX−XXX

Histology of Calvaria. Calvariae were fixed in 4% paraformaldehyde for 2 days and then kept in a decalcifying solution overnight (D0818-1L Sigma-Aldrich) for decalcification. Calvariae were then embedded in paraffin wax, and sections of 5 μm thickness were obtained (Leica Microsystems, Wetzlar, Germany). Tissue sections were deparaffinized in xylene and in graded ethanol series (100, 90, 70, and 50%) and double-stained with hematoxylin and eosin. The hematoxylin and eosin-stained preparations were visualized with a bright-field optical microscope (Evosxl bright-field microscope) at 20× magnification and captured for analysis of calvarial width using Image J software.[46]

Fracture Study. All animal experimental procedures were approved by the Institutional Animal Ethics Committee (IAEC/2020/65). Female SD rats of weight 180 ± 20 g were obtained from the National Laboratory Animal Centre. Animals were treated with good care and were subjected to a 12 h light−dark cycle, appropriate temperature (22−24 °C), humidity (50−60%), and easy access to rodent food and water.

Drill-Hole Defect at the Mid-Diaphysis of the Femur. Fifty adult Sprague-Dawley rats were taken and randomly divided into five groups [Vehicle, PTH (30 μg/kg subcutaneously), and **5e** at 1, 5, and 10 mg/kg] for drill-hole injury. For this, a 1 cm incision in the front skin of the mid-diaphysis of the femur was made to expose the region to be inflicted with injury. Nearby muscles were removed, and the periosteum was stripped off to expose the femoral bone surface. A drill-hole injury was made by inserting a drill bit of diameter 0.8 mm in the anterior portion of the diaphysis, 2 cm above the knee joint. Injury was made in all of the aforementioned groups, and treatment was started from the very next day and continued for 14 days. After 2 weeks, animals were euthanized and femurs were collected for measurement of bone microarchitectural parameters and dynamic histomorphometric study at the drill-hole site.[47]

Fracture Site Bone Regeneration. Each animal was given calcein (20 mg/kg body weight) intraperitonially, 24 h before autopsy. Bones were embedded in an acrylic material, and 50 μm sections were cut using an Isomet bone cutter and photographs were taken under a confocal microscope aided with appropriate filters. The intensity of calcein binding at the fracture site, which is indicative of new mineral deposition, was calculated using Image J software.[48]

To quantify the microarchitecture of callus formed in the drill hole, μCT analysis was performed, using a Sky Scan 1276 CT scanner (Aartselaar, Belgium). Soft tissues were removed carefully without disturbing the callus of the bone and scanned using an X-ray source of 70 kV, 200 mA with a pixel size of 18 mm. The images were reconstructed using Sky Scan Nrecon software. The region of interest (ROI) was drawn around the callus area, and analysis was performed using CTAn software. Microarchitectural parameters including bone volume fraction (BV/TV), trabecular thickness (Tb.Th), and trabecular number (Tb.N) were quantified.[49]

Quantitative Real-Time PCR (qPCR). Three femoral specimens from each group were used to evaluate the mRNA expressions in the callus region by quantitative real-time polymerase chain reactions (RT-PCRs). The drilled regions, exhibiting newly formed callus, were excised as much free from the bone part by a surgical sterilized scalpel. The piece of bone was frozen and powdered in liquid nitrogen using a mortar and pestle. Total RNA was isolated using QIAazol (Qiagen) according to the manufacturer's protocol. The concentration and the purity of RNA were determined by measuring the absorbance at 260/280 nm using a spectrophotometer (NANO-Drop). Further, cDNA was synthesized by a high-capacity cDNA reverse transcription kit with random primers. Gene expressions of OCN and Col1 were assessed using Power up SYBR Green in Applied BiosystemQuantstudio 3 RT-PCR. GAPDH was taken as an internal control.[50]

Histology at the Fracture Site. Femur bones with drill-hole injury were dissected out and cleaned. Bones were fixed in 4% paraformaldehyde for 48 h and then transferred to 70% isopropanol for another 48 h. Bones were then decalcified in a decalcifying solution (Sigma-Aldrich) for 4 days and subsequently embedded in paraffin. For histological analysis of the bone (hard callus) at the fracture site, sections of 5 μm size were cut through transversely. Paraffin sections were dewaxed, rehydrated, stained with hematoxylin and eosin, dehydrated, and mounted. For the analysis of soft callus at the fracture site, sections of 5 μm were cut and double-stained with toluidine blue and fast green. Representative images of the stained sections were selected for observation.

Statistical Analysis. All experiments were performed three times, independently. Data are expressed as mean ± SE. One-way analysis of variance (ANOVA) was used for experiments with multiple comparisons followed by Newman−Keul's test of significance using Graph Pad Prism v.5. Data were presented as the mean ± SE, $^{*}p < 0.05$, $^{**}p < 0.01$, $^{***}p < 0.001$ versus the vehicle group.

LCMS/MS Conditions for In Vivo and In Vitro PK Sample Analysis. The method of compound **5e** was developed using API3200 (Applied Biosystem, MDS Sciex, Toronto, Canada) mass spectroscopy connected with a Waters HPLC system consisting of a Waters 2707 autosampler with Waters Milford USA (quaternary pump-600) for the analysis of *in vitro* and *in vivo* study samples. The processed samples were injected into HPLC (injection volume, 20 μL), and a chromatographic resolution was obtained by the Water symmetry shield C18 column (150 mm × 4.6 mm × 5 μm) attached with a C18 guard column. The isocratic mode was applied for sample elution, and the mobile phase ratio was 90:10 v/v (0.1% formic acid in total distilled water (TDW)/acetonitrile (ACN)) at a flow rate of 0.7 mL/min. Analyte detection was performed using an electrospray ionization source (ESI) in the positive mode, and 4000 ion spray voltage was applied. Compound-dependent parameters such as declustering potential, collision energy, and cell exit potential were set to 92.1, 41.63, and 2, respectively. Multiple reaction monitoring (MRM) modes were used to detect and quantify the analyte as well as IS (carbamezapine) using a precursor → product ion combination of 464.1/195.0 and 237.2/194, respectively.

In Vitro SGF, SIF, and Plasma Stability. The SIF, SGF, and rat plasma stability studies of compound **5e** were performed at 1 μm/mL in triplicate. SGF and SIF were prepared as per the USP guideline.[51] In brief, SGF, SIF, and plasma were taken in glass vials separately and preincubated in a shaking water bath at 37 °C for 10 min. Further, the aliquots of the analyte were spiked separately in both the fluids and 100 μL of the sample was withdrawn at each time point (0, 5, 10, 20, 30, and 60 min). Further, each sample was quenched with acetonitrile (1:3) v/v followed by vortex and centrifugation at 5 min and 12 000 rpm for 10 min, respectively. Finally, 100 μL of the supernatant was collected and loaded in LCMS/MS for analysis.

In Vitro Microsomal Stability. Rat liver microsomes were used for microsomal stability of the analyte, and the study was conducted in triplicate. In brief, 886.5 μL of tris buffer (50 mM, pH 7.4), magnesium chloride (500 mM), RLM protein (0.25 mg/mL), and drug (1 μm/mL) was spiked in each glass test tube separately and preincubated at 37 °C for 10 min. Positive and negative controls were also done for validation and microsomal activity. After preincubation, NADPH (40 mM) was added to each vial to initiate the reaction. The reaction was terminated by adding acetonitrile (200 μL) in each sample (100 μL collection volume) at each time point (0, 5, 10, 20, 30, 40, and 60 min). Finally, the quenched sample was vortexed and centrifuged for 5 min and at 12 000 rpm for 10 min, respectively, and load into LCMS/MS for further analysis.

In Vivo Pharmacokinetic Study. *In vivo* oral pharmacokinetic study of the compound was performed in male SD rats (n = 3). The compound was administered at 5 mg/kg dose through oral gavage to each rat. The formulation was formulated in 0.5 per cent sodium CMC solution in the form of an oral suspension. The blood was collected in microcentrifuge tubes containing heparin at 0.083, 0.25, 0.5, 1, 2, 4, 6, 8, 10, 12, 16, and 24 h after dosing. Before blood collection, each animal was anesthetized using light ether anesthesia. Plasma was collected from blood by centrifugation at 5000 rpm for 20 min and stored at −80 °C until bioanalysis. Protein precipitation technique was used to extract the compound from plasma using acetonitrile (300 μL/100 μL plasma) containing carbamezapine as the internal standard. Finally, the supernatant was collected and injected into LCMS/MS.

Data Analysis. The percentage of the analyte remaining intact at different time intervals after incubation was determined by eq 1, and the graph was plotted between the normal logarithmic of the compound

https://doi.org/10.1021/acs.jmedchem.1c00112
J. Med. Chem. XXXX, XXX, XXX−XXX

remaining over time.[52,53] The curve slope was defined as a depletion rate constant K (min^{-1}). The half-life ($t_{1/2}$) and *in vitro* intrinsic clearance (CL_{ins}) were determined by eqs 2 and 3, respectively.

$$\%\ \text{drug remaining} = (\text{concentration of drug after incubation} / \text{concentration of drug before incubation}) \times 100 \quad (1)$$

$$\text{half life } (t_{1/2}) = 0.693/K \quad (2)$$

$$\text{intrinsic clearance } (CL_{ins}) = K \times \text{volume of incubation } (\mu L) / \text{amount of protein incubated } (mg) \quad (3)$$

■ ASSOCIATED CONTENT

Supporting Information

The Supporting Information is available free of charge at https://pubs.acs.org/doi/10.1021/acs.jmedchem.1c00112.

^{1}H NMR and ^{13}C NMR spectra of all compounds (PDF)

Molecular formula strings (CSV)

■ AUTHOR INFORMATION

Corresponding Authors

Ritu Trivedi − *Division of Endocrinology and Centre for Research on ASTHI, CSIR-Central Drug Research Institute, Lucknow 226031, India; Academy of Scientific and Innovative Research (AcSIR), Ghaziabad 201002 U.P., India*; Phone: +91-0522-2772450; Email: ritu_trivedi@cdri.res.in

Koneni V. Sashidhara − *Medicinal and Process Chemistry Division, CSIR-Central Drug Research Institute, Lucknow 226031, India; Sophisticated Analytical Instrument Facility & Research, CSIR-Central Drug Research Institute, Lucknow 226031 U.P., India; Academy of Scientific and Innovative Research (AcSIR), Ghaziabad 201002 U.P., India*; orcid.org/0000-0002-8339-568X; Phone: +91-522-2772450; Email: kv_sashidhara@cdri.res.in; Fax: +91-522-2771942/2771970

Authors

Alka Raj Pandey − *Medicinal and Process Chemistry Division, CSIR-Central Drug Research Institute, Lucknow 226031, India; Academy of Scientific and Innovative Research (AcSIR), Ghaziabad 201002 U.P., India*

Divya Rai − *Division of Endocrinology and Centre for Research on ASTHI, CSIR-Central Drug Research Institute, Lucknow 226031, India; Academy of Scientific and Innovative Research (AcSIR), Ghaziabad 201002 U.P., India*

Suriya Pratap Singh − *Medicinal and Process Chemistry Division, CSIR-Central Drug Research Institute, Lucknow 226031, India*

Ashish Kumar Tripathi − *Division of Endocrinology and Centre for Research on ASTHI, CSIR-Central Drug Research Institute, Lucknow 226031, India*

Anirban Sardar − *Division of Endocrinology and Centre for Research on ASTHI, CSIR-Central Drug Research Institute, Lucknow 226031, India; Academy of Scientific and Innovative Research (AcSIR), Ghaziabad 201002 U.P., India*

Alisha Ansari − *Medicinal and Process Chemistry Division, CSIR-Central Drug Research Institute, Lucknow 226031, India; Academy of Scientific and Innovative Research (AcSIR), Ghaziabad 201002 U.P., India*

Anjali Mishra − *Pharmacokinetics and Metabolism Division, CSIR-Central Drug Research Institute, Lucknow 226031, India; Academy of Scientific and Innovative Research (AcSIR), Ghaziabad 201002 U.P., India*

Sudha Bhagwati − *Molecular and Structural Biology Division, CSIR-Central Drug Research Institute, Lucknow 226031, India*

Rabi Sankar Bhatta − *Pharmacokinetics and Metabolism Division, CSIR-Central Drug Research Institute, Lucknow 226031, India*; orcid.org/0000-0003-4844-2388

Mohammad Imran Siddiqi − *Molecular and Structural Biology Division, CSIR-Central Drug Research Institute, Lucknow 226031, India*; orcid.org/0000-0001-5655-5484

Naibedya Chattopadhyay − *Division of Endocrinology and Centre for Research on ASTHI, CSIR-Central Drug Research Institute, Lucknow 226031, India; Academy of Scientific and Innovative Research (AcSIR), Ghaziabad 201002 U.P., India*; orcid.org/0000-0003-2473-0246

Complete contact information is available at: https://pubs.acs.org/10.1021/acs.jmedchem.1c00112

Author Contributions

$^{\nabla}$A.R.P. and D.R. contributed equally.

Notes

The authors declare no competing financial interest.

■ ACKNOWLEDGMENTS

The authors are thankful to Director, CSIR-CDRI, for providing necessary research facilities. A.R.P. and A.M. are thankful to the Department of Science and Technology for the Inspire fellowship. D.R. and A.K.T. acknowledge AcSIR, New Delhi, and A.A., D.R., and S.B. acknowledge UGC, New Delhi, for their research fellowships. The authors acknowledge Dr. Chandra Bhushan Tripathi for helping in chiral separation of the compound. The authors are also thankful to the in-house Sophisticated Analytical Instrumentation Facility & Research (SAIF & R) for providing the required spectral data. This manuscript has CDRI Communication no. 10279.

■ ABBREVIATIONS USED

ALP, alkaline phosphatase; BFR, bone formation rate; BMP-2, bone morphogenic protein 2; GAPDH, glyceraldehyde 3-phosphate dehydrogenase; IAEC, Institutional Animal Ethics Committee; MAR, mineral appositional rate; PTH, parathyroid hormone; qPCR, quantitative real-time polymerase chain reaction; RCO, rat calvarial osteoblast; RUNX2, runt-related transcription factor 2; Col1, collagen 1; OCN, osteocalcin; BV/TV, bone volume/tissue fraction; Tb.Th, trabecular thickness; Tb.N, trabecular number; SAR, structure−activity relationship; SERMs, selective estrogen receptor modulators; NMR, nuclear magnetic resonance; HPLC, high-performance liquid chromatography; EC_{50}, half-maximal effective concentration; E_{max}, maximum efficacy; MTT, 3-(4,5-dimethylthiazol-2-yl)-2,5-diphenyltetrazolium bromide; SIF, simulated intestinal fluid; SGF, simulated gastric fluid; NADPH, nicotinamide adenine dinucleotide phosphate; RLM, rat liver microsomes; CL_{int}, intrinsic clearance; AUC, area under the curve; $t_{1/2}$, half-time; C_{max}, maximum concentration; V_d, volume of distribution; Cl, clearance; MRT, mean resident time; MRM, multiple reaction monitoring; CPC, cetylpyridinium chloride; PNPP, *p*-nitrophenylphosphate; ESI, electrospray ionization source

REFERENCES

(1) Sashidhara, K. V.; Kumar, M.; Khedgikar, V.; Kushwaha, P.; Modukuri, R. K.; Kumar, A.; Gautam, J.; Singh, D.; Sridhar, B.; Trivedi, R. Discovery of coumarin−dihydropyridine hybrids as bone anabolic agents. *J. Med. Chem.* **2013**, *56*, 109−122.

(2) Kushwaha, P.; Tripathi, A. K.; Gupta, S.; Kothari, P.; Upadhyay, A.; Ahmad, N.; Sharma, T.; Siddiqi, M. I.; Trivedi, R.; Sashidhara, K. V. Synthesis and study of benzofuran-pyran analogs as bmp-2 targeted osteogenic agents. *Eur. J. Med. Chem.* **2018**, *156*, 103−117.

(3) Reginster, J.-Y.; Burlet, N. Osteoporosis: A still increasing prevalence. *Bone* **2006**, *38*, 4−9.

(4) Fu, H.; Zhou, Y.-R.; Bao, B.; Jia, M.; Zhao, Y.; Zhang, L.; Li, J.; He, H.; Zhou, X. Tryptophan hydroxylase 1 (Tph-1)-targeted bone anabolic agents for osteoporosis. *J. Med. Chem.* **2014**, *57*, 4692−4709.

(5) Balaramnavar, V. M.; Khan, I. A.; Siddiqui, J. A.; Khan, M. P.; Chakravarti, B.; Sharan, K.; Swarnkar, G.; Rastogi, N.; Siddiqui, H. H.; Mishra, D. P.; Chattopadhyay, N.; Saxena, A. K. Identification of novel 2-((1-(benzyl(2-hydroxy-2-phenylethyl)amino)-1-oxo-3-phenylpropan-2-yl)carbamoyl)benzoic acid analogues as BMP-2 stimulators. *J. Med. Chem.* **2012**, *55*, 8248−8259.

(6) Modukuri, R. K.; Choudhary, D.; Gupta, S.; Rao, K. B.; Adhikary, S.; Sharma, T.; Siddiqi, M. I.; Trivedi, R.; Sashidhara, K. V. benzofuran-dihydropyridine hybrids: a new class of potential bone anabolic agents. *Bioorg. Med. Chem.* **2017**, *25*, 6450−6466.

(7) Bhattacharyya, S.; Pal, S.; Chattopadhyay, N. Abaloparatide, the second generation osteoanabolic drug: Molecular mechanisms underlying its advantages over the first-in-class teriparatide. *Biochem. Pharmacol.* **2019**, *166*, 185−191.

(8) Bhattacharyya, S.; Pal, S.; Chattopadhyay, N. Targeted inhibition of sclerostin for post-menopausal osteoporosis therapy: A critical assessment of the mechanism of action. *Eur. J. Pharmacol.* **2018**, *826*, 39−47.

(9) Lin, S.-Y.; Kang, L.; Wang, C.-Z.; Huang, H.; Cheng, T.-L.; Huang, H.-T.; Lee, M.-J.; Lin, Y.-S.; Ho, M.-L.; Wang, G.-J.; Chen, C.-H. (−)-Epigallocatechin-3-Gallate (EGCG) Enhances osteogenic differentiation of human bone marrow mesenchymal stem cells. *Molecules* **2018**, *23*, 3221−3232.

(10) Chauhan, S.; Sharma, A.; Upadhyay, N. K.; Singh, G.; Lal, U. R.; Goyal, R. In-Vitro Osteoblast Proliferation and in-Vivo Anti-osteoporotic activity of *Bombax ceiba* with quantification of lupeol, gallic acid and β-sitosterol by HPTLC and HPLC. *BMC Complementary Altern. Med.* **2018**, *18*, No. 233.

(11) Lu, Z.; Nie, G.; Belton, P. S.; Tang, H.; Zhao, B. Structure−Activity Relationship analysis of antioxidant ability and neuroprotective effect of gallic acid derivatives. *Neurochem. Int.* **2006**, *48*, 263−274.

(12) Huang, L.; Jin, P.; Lin, X.; Lin, C.; Zheng, L.; Zhao, J. Beneficial effects of sulfonamide-based gallates on osteoblasts in vitro. *Mol. Med. Rep.* **2017**, *15*, 1149−1156.

(13) Jin, P.; Liao, L.; Lin, X.; Guo, Q.; Lin, C.; Wu, H.; Zheng, L.; Zhao, J. stimulating effect of a novel synthesized sulfonamido-based gallate ZXHA-TC on primary osteoblasts. *Yonsei Med. J.* **2015**, *56*, 760−771.

(14) Konishi, Y.; Hitomi, Y.; Yoshioka, E. Intestinal absorption of p-coumaric and gallic acids in rats after oral administration. *J. Agric. Food Chem.* **2004**, *52*, 2527−2532.

(15) Song, N.; Zhao, Z.; Ma, X.; Sun, X.; Ma, J.; Li, F.; Sun, L.; Lv, J. Naringin promotes fracture healing through stimulation of angiogenesis by regulating the vegf/vegfr-2 signaling pathway in osteoporotic rats. *Chem. Biol. Interact.* **2017**, *261*, 11−17.

(16) Liu, H.; Dong, Y.; Gao, Y.; Zhao, L.; Cai, C.; Qi, D.; Zhu, M.; Zhao, L.; Liu, C.; Guo, F.; Xiao, J.; Huang, H. Hesperetin suppresses RANKL-induced osteoclastogenesis and ameliorates lipopolysaccharide-induced bone loss. *J. Cell. Physiol.* **2019**, *234*, 11009−11022.

(17) Afridi, R.; Khan, A. U.; Khalid, S.; Shal, B.; Rasheed, H.; Ullah, M. Z.; Shehzad, O.; Kim, Y. S.; Khan, S. Anti-hyperalgesic properties of a flavanone derivative poncirin in acute and chronic inflammatory pain models in mice. *BMC Pharmacol. Toxicol.* **2019**, *20*, No. 57.

(18) Safavi, M.; Esmati, N.; Ardestani, S. K.; Emami, S.; Ajdari, S.; Davoodi, J.; Shafiee, A.; Foroumadi, A. halogenated flavanones as potential apoptosis-inducing agents: synthesis and biological activity evaluation. *Eur. J. Med. Chem.* **2012**, *58*, 573−580.

(19) Bano, S.; Javed, K.; Ahmad, S.; Rathish, I. G.; Singh, S.; Chaitanya, M.; Arunasree, K. M.; Alam, M. S. Synthesis of some novel chalcones, flavanones and flavones and evaluation of their anti-inflammatory activity. *Eur. J. Med. Chem.* **2013**, *65*, 51−59.

(20) Chandrappa, S.; Vinaya, K.; Ramakrishnappa, T.; Rangappa, K. An efficient method for aryl nitro reduction and cleavage of azo compounds using Iron powder/calcium chloride. *Synlett* **2010**, *2010*, 3019−3022.

(21) Gao, Y.; Mao, Y.; Zhang, B.; Zhan, Y.; Huo, Y. Regioselective nitration of anilines with $Fe(NO_3)_3{\cdot}9H_2O$ as a promoter and a nitro source. *Org. Biomol. Chem.* **2018**, *16*, 3881−3884.

(22) Lévai, A. Utilization of the chiroptical spectroscopies for the structure elucidation of flavanoids of flavanoids and related benzopyran derivatives. *Acta Chim. Slov.* **1998**, *45*, 267−284.

(23) Whyte, M. P. Hypophosphatasia and the role of alkaline phosphatase in skeletal mineralization. *Endocr. Rev.* **1994**, *15*, 439−461.

(24) Kaul, H.; Hall, B. K.; Newby, C.; Ventikos, Y. Synergistic activity of polarised osteoblasts inside condensations cause their differentiation. *Sci. Rep.* **2015**, *5*, No. 11838.

(25) Wang, Y.-H.; Liu, Y.; Maye, P.; Rowe, D. W. Examination of mineralized nodule formation in living osteoblastic cultures using fluorescent dyes. *Biotechnol. Prog.* **2006**, *22*, 1697−1701.

(26) Komori, T. Regulation of proliferation, differentiation and functions of osteoblasts by RUNX2. *Int. J. Mol. Sci.* **2019**, *20*, 1694−1705.

(27) Huang, W. Signaling and transcriptional regulation in osteoblast commitment and differentiation. *Front. Biosci.* **2007**, *12*, 3068−3092.

(28) Khan, M. P.; Khan, K.; Yadav, P. S.; Singh, A. K.; Nag, A.; Prasahar, P.; Mittal, M.; China, S. P.; Tewari, M. C.; Nagar, G. K.; Tewari, D.; Trivedi, A. K.; Sanyal, S.; Bandyopadhyay, A.; Chattopadhyay, N. BMP signaling is required for adult skeletal homeostasis and mediates bone anabolic action of parathyroid hormone. *Bone* **2016**, *92*, 132−144.

(29) Rogers, M. B.; Shah, T. A.; Shaikh, N. N. Turning bone morphogenetic protein 2 (bmp2) on and off in mesenchymal cells. *J. Cell. Biochem.* **2015**, *116*, 2127−2138.

(30) Wang, R. N.; Green, J.; Wang, Z.; Deng, Y.; Qiao, M.; Peabody, M.; Zhang, Q.; Ye, J.; Yan, Z.; Denduluri, S.; Idowu, O.; Li, M.; Shen, C.; Hu, A.; Haydon, R. C.; Kang, R.; Mok, J.; Lee, M. J.; Luu, H. L.; Shi, L. L. Bone morphogenetic protein (BMP) signaling in development and human diseases. *Genes Dis.* **2014**, *1*, 87−105.

(31) Pal, S.; Porwal, K.; Rajak, S.; Sinha, R. A.; Chattopadhyay, N. Selective dietary polyphenols induce differentiation of human osteoblasts by adiponectin receptor 1-mediated reprogramming of mitochondrial energy metabolism. *Biomed. Pharmacother.* **2020**, *127*, 110207.

(32) Tripathi, A. K.; Rai, D.; Kothari, P.; Kushwaha, P.; Sinha, S.; Sardar, A.; Sashidhara, K. V.; Trivedi, R. Benzofuran pyran compound rescues rat and human osteoblast from lipotoxic effect of palmitate by inhibiting lipid biosynthesis and promoting stabilization of RUNX2. *Toxicol. In Vitro* **2020**, *66*, No. 104872.

(33) Ferron, M.; Lacombe, J.; Germain, A.; Oury, F.; Karsenty, G. GGCX and VKORC1 inhibit osteocalcin endocrine functions. *J. Cell Biol.* **2015**, *208*, 761−776.

(34) Rice, R.; Rice, D. P. C.; Olsen, B. R.; Thesleff, I. Progression of calvarial bone development requires foxc1 regulation of Msx2 and Alx4. *Dev. Biol.* **2003**, *262*, 75−87.

(35) Kumar, P.; Kushwaha, P.; Ahmad, N.; Maurya, S. W.; Dev, K.; Khedgikar, V.; Siddiqui, I. R.; Trivedi, R.; Maurya, R. Design and synthesis of dalbergin analogues and evaluation of anti-osteoporotic activity. *Bioorg. Med. Chem. Lett.* **2017**, *27*, 1765−1775.

(36) Porwal, K.; Pal, S.; Tewari, D.; Pal China, S.; Singh, P.; Chandra Tewari, M.; Prajapati, G.; Singh, P.; Cheruvu, S.; Khan, Y. A.; Sanyal, S.; Gayen, J. R.; Ampapathi, R.; Mridha, A. R.; Chattopadhyay, N. Increased bone marrow-specific adipogenesis by clofazimine causes impaired fracture healing, osteopenia, and osteonecrosis without extraskeletal effects in rats. *Toxicol. Sci.* **2019**, *172*, 167−180.

https://doi.org/10.1021/acs.jmedchem.1c00112
J. Med. Chem. XXXX, XXX, XXX−XXX

(37) Bissinger, O.; Götz, C.; Wolff, K.-D.; Hapfelmeier, A.; Prodinger, P. M.; Tischer, T. Fully automated segmentation of callus by micro-ct compared to biomechanics. *J. Orthop. Surg. Res.* **2017**, *12*, No. 108.
(38) Kostenuik, P.; Mirza, F. M. Fracture healing physiology and the quest for therapies for delayed healing and nonunion. *J. Orthop. Res.* **2017**, *35*, 213−223.
(39) Khan, K.; Pal, S.; Yadav, M.; Maurya, R.; Trivedi, A. K.; Sanyal, S.; Chattopadhyay, N. Prunetin Signals via G-Protein-Coupled Receptor, GPR30(GPER1): Stimulation of adenylyl cyclase and camp-mediated activation of mapk signaling induces RUNX2 expression in osteoblasts to promote bone regeneration. *J. Nutr. Biochem.* **2015**, *26*, 1491−1501.
(40) Anderson, A. M.; Hastings, G. W.; Fisher, T. R.; Ross, E. R. S.; Shuttleworth, A. Collagen types present at human fracture sites-a preliminary report. *Injury* **1986**, *17*, 78−80.
(41) Nakamura, A.; Dohi, Y.; Akahane, M.; Ohgushi, H.; Nakajima, H.; Funaoka, H.; Takakura, Y. Osteocalcin secretion as an early marker of in vitro osteogenic differentiation of rat mesenchymal stem cells. *Tissue Eng., Part C* **2009**, *15*, 169−180.
(42) Zieba, J.; Munivez, E.; Castellon, A.; Jiang, M.; Dawson, B.; Ambrose, C. G.; Lee, B. Fracture healing in collagen-related preclinical models of osteogenesis imperfecta. *J. Bone Miner. Res.* **2020**, *35*, 1132−1148.
(43) Wen, X.; Walle, T. Methylation Protects dietary flavonoids from rapid hepatic metabolism. *Xenobiotica* **2006**, *36*, 387−397.
(44) Kothari, P.; Sinha, S.; Sardar, A.; Tripathi, A. K.; Girme, A.; Adhikary, S.; Singh, R.; Maurya, R.; Mishra, P. R.; Hingorani, L.; Trivedi, R. Inhibition of cartilage degeneration and subchondral bone deterioration by spinacia oleracea in human mimic of ACLT-induced osteoarthritis. *Food Funct.* **2020**, *11*, 8273−8285.
(45) Karvande, A.; Kushwaha, P.; Ahmad, N.; Adhikary, S.; Kothari, P.; Tripathi, A. K.; Khedgikar, V.; Trivedi, R. Glucose dependent MiR-451a expression contributes to parathyroid hormone mediated osteoblast differentiation. *Bone* **2018**, *117*, 98−115.
(46) Hwang, J.-H.; Cha, P.-H.; Han, G.; Bach, T. T.; Min, D. S.; Choi, K.-Y. Euodia sutchuenensis dode extract stimulates osteoblast differentiation via wnt/β-catenin pathway activation. *Exp. Mol. Med.* **2015**, *47*, e152.
(47) Pal, S.; Porwal, K.; Singh, H.; Malik, M. Y.; Rashid, M.; Kulkarni, C.; Khan, Y.; Jagavelu, K.; Wahajuddin, M.; Chattopadhyay, N. Reversal of osteopenia in ovariectomized rats by pentoxifylline: evidence of osteogenic and osteo-angiogenic roles of the drug. *Calcif. Tissue Int.* **2019**, *105*, 294−307.
(48) Adhikary, S.; Choudhary, D.; Ahmad, N.; Kumar, S.; Dev, K.; Mittapelly, N.; Pandey, G.; Mishra, P. R.; Maurya, R.; Trivedi, R. Dried and free flowing granules of spinacia oleracea accelerate bone regeneration and alleviate postmenopausal osteoporosis. *Menopause* **2017**, *24*, 686−698.
(49) Pal, S.; Mittapelly, N.; Husain, A.; Kushwaha, S.; Chattopadhyay, S.; Kumar, P.; Ramakrishna, E.; Kumar, S.; Maurya, R.; Sanyal, S.; Gayen, J. R.; Mishra, P. R.; Chattopadhyay, N. A butanolic fraction from the standardized stem extract of cassia occidentalis l delivered by a self-emulsifying drug delivery system protects rats from glucocorticoid-induced osteopenia and muscle atrophy. *Sci. Rep.* **2020**, *10*, No. 195.
(50) Ahmad, N.; Chillara, R.; Kushwaha, P.; Khedgikar, V.; Karvande, A.; Choudhary, D.; Adhikary, S.; Maurya, R.; Trivedi, R. Evaluation of anti-osteoporotic activity of butanolic fraction from passiflora foetida in ovariectomy-induced bone loss in mice. *Biomed. Pharmacother.* **2017**, *88*, 804−813.
(51) XXIV, U.P. The United State of Pharmacopoeia Convention: Rockville, Maryland, 2000; p 185.
(52) Chhonker, Y. S.; Sleightholm, R. L.; Murry, D. J. Bioanalytical method development and validation of moxidectin in plasma by LCMS/MS: Application to *in vitro* metabolism. *Biomed. Chromatogr.* **2019**, *33*, No. e4389.
(53) Liu, H.; Huang, Z.; Li, H.; Zhang, Q.; Tan, X.; Lu, F.; Li, S. Characterization of preclinical *in vitro* and *in vivo* pharmacokinetics properties for kbp-7018, a new tyrosine kinase inhibitor candidate for treatment of idiopathic pulmonary fibrosis. *Drug Des., Dev. Ther.* **2015**, *9*, 4319−4328.

https://doi.org/10.1021/acs.jmedchem.1c00112
J. Med. Chem. XXXX, XXX, XXX−XXX